Glycobiology vol. 23 no. 6 pp. 690–708, 2013
doi:10.1093/glycob/cwt009
Advance Access publication on February 7, 2013

A non-enzymatic function of Golgi glycosyltransferases: Mediation of Golgi fragmentation by interaction with non-muscle myosin IIA

Armen Petrosyan[2,3] and Pi-Wan Cheng[1,2,3,4]

[2]Department of Research Service, VA Nebraska-Western Iowa Health Care System, Omaha, NE 68105 USA; [3]Department of Biochemistry and Molecular Biology, College of Medicine; and [4]Eppley Institute for Research in Cancer and Allied Diseases, University of Nebraska Medical Center, 985870 Nebraska Medical Center, Omaha, NE 68198-5870 USA

Received on December 26, 2012; revised on January 29, 2013; accepted on February 5, 2013

The Golgi apparatus undergoes morphological changes under stress or malignant transformation, but the precise mechanisms are not known. We recently showed that non-muscle myosin IIA (NMIIA) binds to the cytoplasmic tail of Core 2 N-acetylglucosaminyltransferase mucus-type (C2GnT-M) and transports it to the endoplasmic reticulum for recycling. Here, we report that Golgi fragmentation induced by brefeldin A (BFA) or coatomer protein (β-COP) knockdown (KD) in Panc1-bC2GnT-M (c-Myc) cells is accompanied by the increased association of NMIIA with C2GnT-M and its degradation by proteasomes. Golgi fragmentation is prevented by inhibition or KD of NMIIA. Using multiple approaches, we have shown that the speed of BFA-induced Golgi fragmentation is positively correlated with the levels of this enzyme in the Golgi. The observation is reproduced in LNCaP cells which express high levels of two endogenous glycosyltransferases—C2GnT-L and β-galactoside α2,3 sialyltransferase 1. NMIIA is found to form complexes with these two enzymes but not Golgi matrix proteins. The KD of both enzymes or the prevention of Golgi glycosyltransferases from exiting endoplasmic reticulum reduced Golgi-associated NMIIA and decreased the BFA-induced fragmentation. Interestingly, the fragmented Golgi detected in colon cancer HT-29 cells can be restored to a compact morphology after inhibition or KD of NMIIA. The Golgi disorganization induced by the microtubule or actin destructive agent is NMIIA-independent and does not affect the levels of glycosyltransferases. We conclude that NMIIA interacts with Golgi residential but not matrix proteins, and this interaction is responsible for Golgi fragmentation induced by β-COP KD or BFA treatment. This is a novel non-enzymatic function of Golgi glycosyltransferases.

[1]To whom correspondence should be addressed: Tel: +1-402-559-5776; Fax: +1-402-559-6650; e-mail: pcheng@unmc.edu

Keywords: brefeldin A / glycosyltransferase / non-muscle myosin IIA / restoration of fragmented Golgi in cancer cells to a compact phenotype / stress-induced Golgi fragmentation

Introduction

The Golgi apparatus is a dynamic membrane complex consisting of pancake-like cisternal stacks localized to the perinuclear region of the cell (Munro 2011). One main function of the Golgi is to elaborate conjugated glycans by a huge family of glycosyltransferases (Morré and Mollenhauer 2009). Golgi glycosyltransferases are type II membrane proteins that contain a short cytoplasmic tail (CT), a transmembrane domain, a short stem and a large C-terminal catalytic region located in the Golgi lumen (Paulson and Colley 1989; Burke et al. 1994). The CT is the primary determinant of the Golgi localization of glycosyltransferases (Grabenhorst and Conradt 1999; Osman et al. 1996; Uliana et al. 2006; Ali et al. 2012) and their vesicular transport between the Golgi apparatus and the endoplasmic reticulum (ER) (Schaub et al. 2006; Okamoto et al. 2008; Petrosyan, Ali, Verma, et al. 2012). Glycosyltransferases also are involved in the maintenance of the Golgi architecture. For example, the mutation of the membrane-spanning domain of an *N*-acetylglucosaminyltransferase caused a dramatic effect on the Golgi morphology (Nilsson et al. 1996). In addition, the CT of a galactosyltransferase binds to cytoskeleton to stabilize the Golgi (Yamaguchi and Fukuda 1995; Wassler et al. 2001).

The intracellular vesicular transport is powered by molecular motors. To date, a number of motor proteins have been shown to be associated with the Golgi apparatus (Allan et al. 2002). About 27 years ago, non-muscle myosin was identified in the *trans*-cisternae of the Golgi (Bendayan 1985). Recently, it has been shown that Golgi phosphoprotein 3 directly binds to phosphatidylinositide-4-phosphate in the Golgi and Myosin XVIIIA in the cytoplasm, and this linkage provides a mechanism required for efficient tubule and vesicle formation from *trans*-Golgi (Dippold et al. 2009). Non-muscle myosin IIA (NMIIA) was found to be dynamically associated with *trans*-Golgi network membranes during the budding and trafficking of a subpopulation of transport vesicles (Ikonen et al. 1997; Müsch et al. 1997; Stow et al. 1998). NMIIs consist of two heavy chains and two pairs of light chains located at the N terminus of the heavy chains (Conti and Adelstein 2008). The N-terminal region contains an ATPase, which provides the

power for vesicular transport, and actin binding sites, which allow the cargo-carrying NMIIA to walk on the actin filaments (Korn and Hammer 1988; Conti and Adelstein 2008). The cargo-binding site has been localized to the C-terminal region of the heavy chain (DePina et al. 2007). Phosphorylation in the rod domain of NMIIA modulates the binding and/or release of NMII from the Golgi, which regulates the extension of Golgi membrane tubules and/or the separation of vesicles from the Golgi complex (Fath 2005). Recently, NMIIs were shown to use the actin cytoskeleton to transport proteins from the Golgi to the ER and be involved in the brefeldin A (BFA)-induced collapse of the Golgi (Duran et al. 2003). Our laboratory (Petrosyan, Ali, Verma, et al. 2012) confirmed and further extended this observation by showing that core 2 *N*-acetylglucosaminyltransferase mucus-type (C2GnT-M), the enzyme that synthesizes all three β6GlcNAc branch structures found in secreted mucins (Ropp et al. 1991; Cheng and Radhakrishnan 2011), utilizes an NMIIA-dependent mechanism for its transport to the ER. Interaction of the C-terminal region of the NMIIA heavy chain with the CT of C2GnT-M was demonstrated by several independent approaches. They include the in vitro pulldown of the recombinant C-terminal region of NMIIA heavy chain or NMIIA from cell lysates using biotinylated CT and yeast two-hybrid analysis. The formation of NMIIA–C2GnT-M complexes was demonstrated by coimmunoprecipitation (Co-IP) and confirmed by confocal microscopy. We also showed that C2GnT-M was degraded by proteasome. Inhibition or knockdown (KD) of NMIIA prevented the BFA-induced Golgi collapse. These data indicate that the association of NMIIA with the CT of Golgi resident proteins such as C2GnT-M is responsible for Golgi remodeling (Petrosyan, Ali, Verma, et al. 2012).

The Golgi apparatus undergoes morphological changes under various conditions, such as cell division, stress, malignant transformation or treatment with various inhibitors (Egea et al. 1993; Kellokumpu et al. 2002; Siddhanta et al. 2003; Hicks and Machamer 2005). However, the precise mechanisms are poorly understood. Because the maintenance of the structure and function of the Golgi apparatus requires a constant supply of Golgi resident proteins from the ER (Ward et al. 2001), and NMIIA controls their exit from the Golgi for recycling (Duran et al. 2003; Vazhappilly et al. 2010; Petrosyan, Ali, Verma, et al. 2012), we chose to investigate the effects of perturbing the intra-Golgi levels of glycosyltransferases on the morphology of the Golgi with or without inhibition or KD of NMIIA. We have found that the deficiency of NMIIA prevents the Golgi morphological changes induced by BFA or KD of β-COP. We propose that NMIIA is a master regulator of Golgi fragmentation, a process requiring interaction of NMIIA with Golgi resident proteins, such as glycosyltransferases. Further, this is a novel non-enzymatic function of Golgi glycosyltransferases. However, NMIIA is not involved in the Golgi disorganization induced by the dissolution of actins or microtubules.

Results

BFA treatment increases C2GnT-M binding to NMIIA and C2GnT-M degradation by the proteasome

We have shown recently that NMIIA is involved in the BFA-induced Golgi-to-ER retrograde transport of Golgi glycosyltransferase, C2GnT-M. Also, we have found that C2GnT-M is degraded by proteasomes, and inhibition of NMIIA blocks C2GnT-M degradation (Petrosyan, Ali, Verma, et al. 2012). Based on observations that BFA treatment causes the proteasome-dependent degradation of Golgi proteins (Dusseljee et al. 1998; Sakata et al. 2001), we examined whether NMIIA directly participates in the BFA-induced proteasome-mediated degradation of Golgi glycosyltransferases and whether NMIIA and C2GnT-M are required for the Golgi collapse caused by BFA treatment. As shown in Figure 1A, the treatment of Panc1-bC2GnT-M (c-Myc) cells with 36 μM BFA for 15 min increased the association of NMIIA with C2GnT-M, demonstrated by pulldown with anti-c-Myc antibodies (Abs) from the cell lysate. BFA treatment also increased the amount of ubiquitinylated C2GnT-M observed upon pulldown (Figure 1A). Double immunofluorescence staining of C2GnT-M and NMIIA showed a significant increase of their colocalization after BFA treatment (Figure 1B). Time course experiments revealed perinuclear colocalization after 5 minutes BFA treatment, and cytoplasmic localization after 20 minutes (Figure 1B). The result was confirmed by increased Mander's overlap coefficients (Figure 1C). The level of C2GnT-M continued to decrease from 15 to 60 min BFA treatment as monitored by confocal immunofluorescence microscopy and western blotting. However, the maximal expression of NMIIA was detected at 45 min (Figure 1D–F). Pretreatment of Panc1-bC2GnT-M (c-Myc) cells with a proteasome inhibitor MG-132, which caused the cytoplasmic accumulation of total and ubiquitinylated C2GnT-M (Petrosyan, Ali, Verma, et al. 2012), prevented the BFA-induced decline in C2GnT-M (Figure 1G–I). The results indicate that BFA treatment increases the interaction of C2GnT-M with NMIIA followed by the proteasomal degradation of C2GnT-M.

We recently showed that NMIIA inhibitor Blebbistatin abolished the colocalization of NMIIA and C2GnT-M at the Golgi periphery and prevented the BFA-induced Golgi collapse (Petrosyan, Ali, Verma, et al. 2012). Blebbistatin can inhibit both NMIIA and NMIIB (Straight et al. 2003), so we used siRNA KD of NMIIA or NMIIB to distinguish which myosin is responsible for the BFA-induced collapse. KD of NMIIA, but not NMIIB, prevented the BFA-induced collapse of the Golgi (Figure S1C). These data are consistent with the observation that NMIIA is distributed throughout the cytoplasm with some localized at the Golgi periphery, whereas the vast majority of NMIIB is localized to the cell periphery (Figure S1A and B). The results fit well with the distinct roles that NMIIA and NMIIB play in vesicular trafficking and cell motility, respectively (Togo and Steinhardt 2004).

The efficiency of BFA-induced Golgi collapse depends on the levels of C2GnT-M in the Golgi

To examine the role of a glycosyltransferase in BFA-induced Golgi fragmentation, we compared the kinetics of the Golgi collapse in BFA-treated HEK293 cells which had transiently expressed wild-type or CT-mutated (WKR→A^4AA^6) C2GnT-M tagged with green fluorescent protein (GFP). We found that the mutation of the CT drastically changed C2GnT-M localization. Although C2GnT-M-WT-GFP colocalized with a Golgi marker Giantin and not an ER marker protein disulfide isomerase (PDI), C2GnT-M-A^4AA^6-GFP

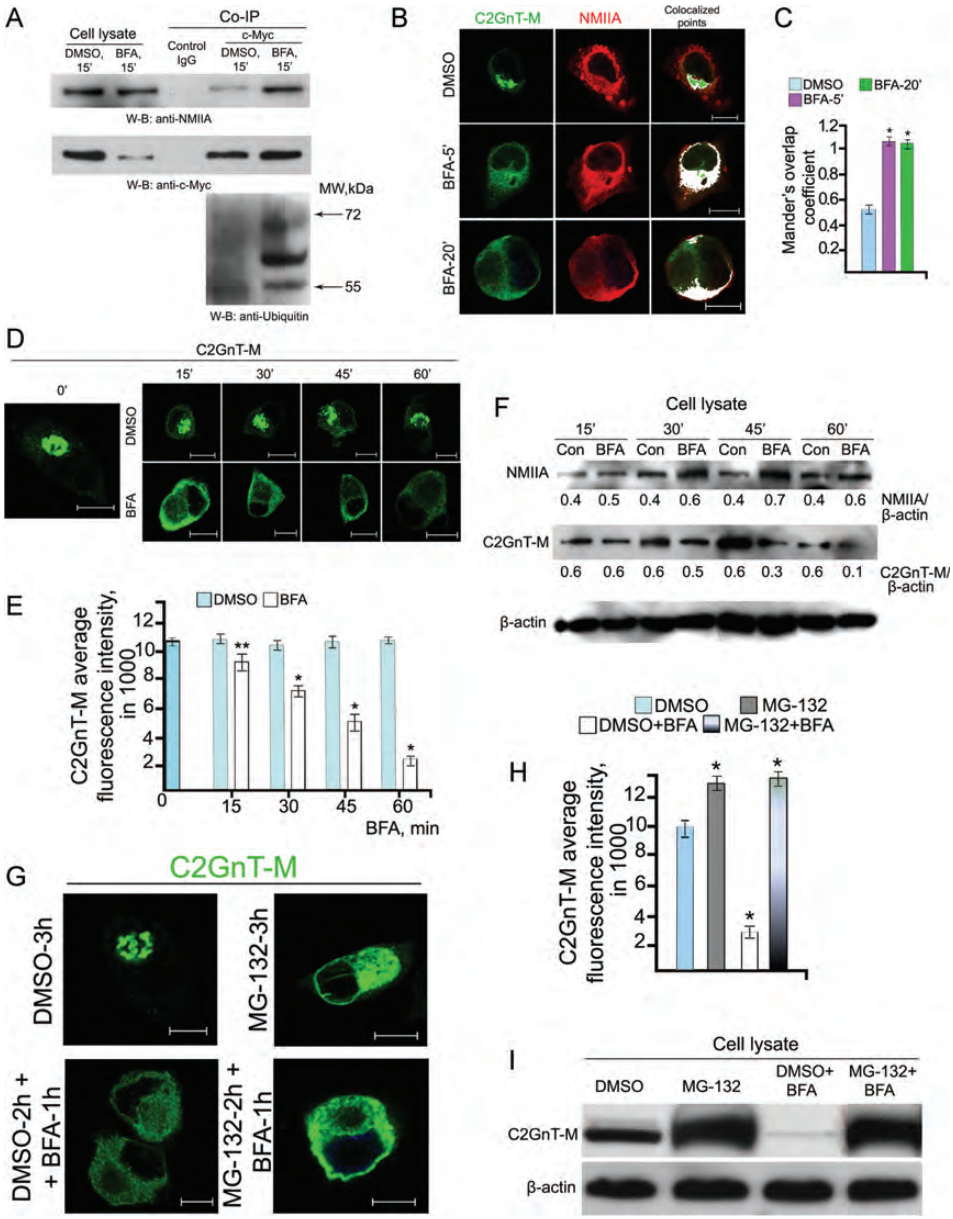

Fig. 1. BFA induces time-dependent proteasome-mediated degradation of C2GnT-M via binding to NMIIA in Panc1-bC2GnT-M (c-Myc) cells. (**A**) NMIIA, c-Myc and Ubiquitin western blots of complexes pulled down with anti-c-Myc Abs from the lysates of cells treated with DMSO or BFA for 15 min. Cell lysate exposed to non-specific IgG served as the negative control. Lysates containing equal amounts of NMIIA were used for Co-IP. (**B** and **C**) Confocal immunofluorescence images of bC2GnT-M and NMIIA in cells ($n = 30$) treated by BFA for 5 or 20 min. BFA treatment substantially increased the Mander's overlap coefficient of C2GnT-M and NMIIA colocalization; $*P < 0.001$ compared with control. (**D** and **E**) BFA treatment for 15–60 min caused a time-dependent decrease in the average fluorescence intensity of bC2GnT-M; $**P < 0.01$; $*P < 0.001$ compared with the control ($n = 30$). The bar at 0 min represents the fluorescence intensity of bC2GnT-M in untreated cells. (**F**) NMIIA and c-Myc western blots of cell lysates from cells treated with 36 μM BFA and the corresponding amount of DMSO (Con). The increase in the expression of NMIIA was detected at 15, 30, 45 and 60 min treatment, whereas C2GnT-M was decreased gradually from 15 to 60 min treatment. Densitometric analysis of proteins is presented below every band. (**G** and **H**) Confocal immunofluorescence images of bC2GnT-M in cells ($n = 30$) treated with DMSO, proteasome inhibitor MG-132, DMSO followed by BFA (DMSO + BFA) or MG-132 followed by BFA (MG-132 + BFA) as described in the *Materials and methods* section. BFA treatment had no effect on the C2GnT-M fluorescence intensity upon pretreatment with MG-132; $*P < 0.001$ for DMSO + BFA vs DMSO, DMSO vs MG-132 and DMSO + BFA vs MG-132 + BFA. (**I**) c-Myc western blots of cell lysates from cells treated with agents described in (**G**). All confocal images were acquired with the same imaging parameters; bars, 10 μm.

mostly overlaid with PDI and not Giantin (Figure 2A and B). Quantification of the cytoplasm/perinuclear area ratio of C2GnT-M in cells ($n = 30$) obtained from three independent experiments confirmed that the amount of C2GnT-M in the ER increased substantially after the triple Ala mutation of the CT (Figure 2C). As expected, extensive Golgi fragmentation was detected after 10 min of BFA treatment of cells expressing wild-type C2GnT-M (Figure 2D). However, only the minimal expansion of the Golgi was observed in cells expressing mutant C2GnT-M-A^4AA^6 (Figure 2D and E). After 15

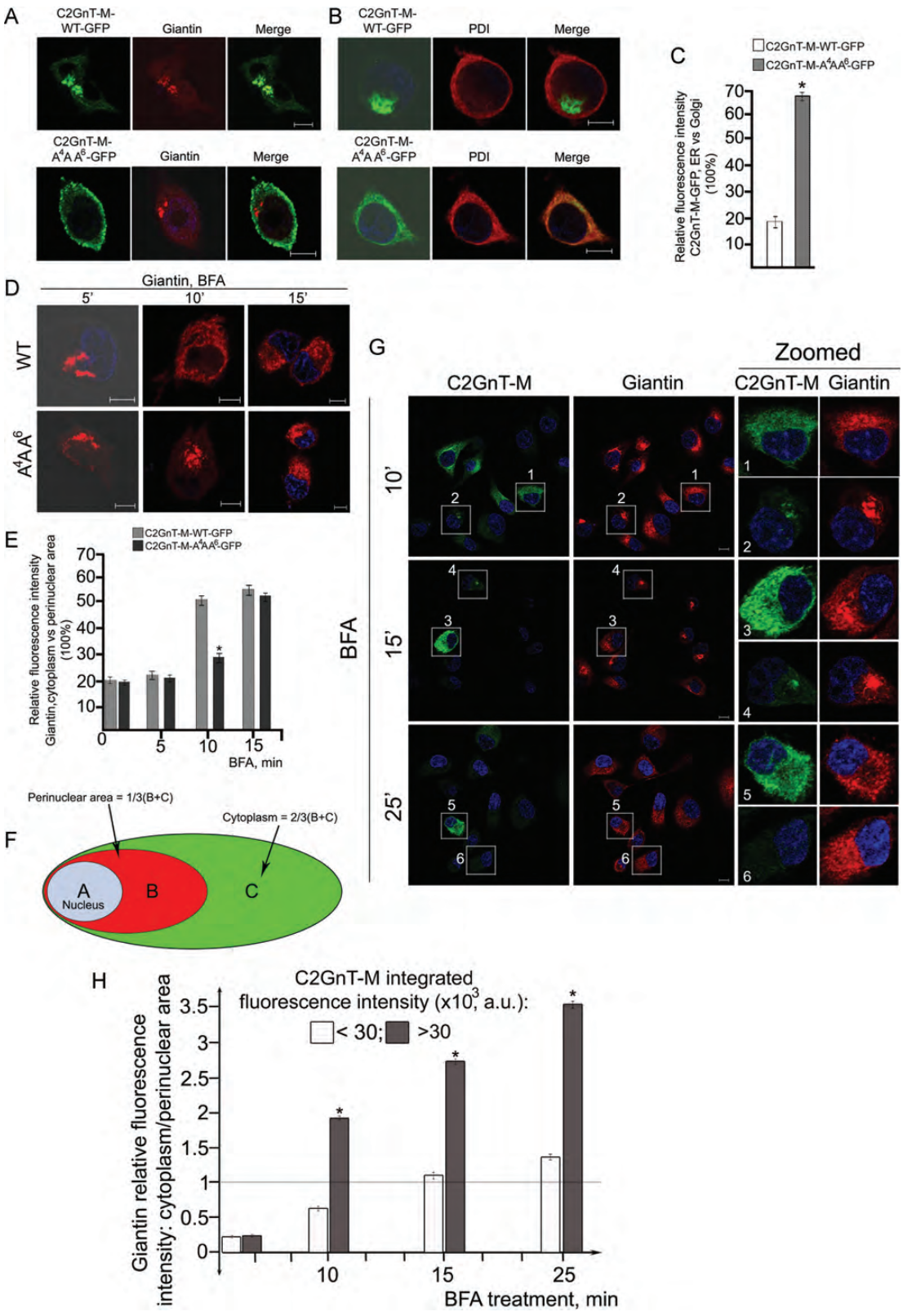

Fig. 2. The efficiency of BFA effects depends on the presence of C2GnT-M in the Golgi. (**A** and **B**) Wild-type C2GnT-M (WT)-GFP was localized primarily to the Golgi (Giantin) in HEK293 cells, while mutant C2GnT-M (A^4AA^6)-GFP was found in the ER (PDI). (**C**) Quantification of the intensity of C2GnT-M-GFP fluorescence in the cytoplasm vs that in the Golgi (=100%). Data were obtained from 30 cells in three independent experiments and expressed as the mean percentage ± SEM; $*P < 0.001$. (**D** and **E**) Time-dependent changes of the intracellular distribution of Giantin in the cells in (A) after BFA treatment. Relative

min of BFA treatment, the Golgi morphology in both cells was similarly expanded.

Panc1-bC2GnT-M cells express heterogeneous levels of bC2GnT-M and were stratified into high (>30 000 a.u. of integrated fluorescence intensity) or low (<30 000 a.u.) C2GnT-M expression. We compared the BFA-induced movement of a Golgi matrix protein Giantin toward the ER as a function of bC2GnT-M levels. We treated these cells with 36 μM BFA for 10, 15 and 25 min and then analyzed the relationship of the C2GnT-M fluorescence intensity with the degree of dispersion of a Golgi matrix protein Giantin between cytoplasm and the perinuclear area where the Golgi is located (Figure 2F–H). The data were obtained from the analysis of 60 cells at every time point from three independent experiments. We found more cytoplasmic distribution of Giantin, i.e. cytoplasm/perinuclear area ratio > 1, in cells that expressed high levels of C2GnT-M vs low levels. As shown in Figure 2G, cells with the high level of C2GnT-M (cells #1, 3 and 5) vs cells expressing the low level of C2GnT-M (cells #2, 4 and 6) showed different sensitivity to BFA action. For example, after 10 min of BFA treatment, in cell #1, Giantin staining was already detected at the cell periphery. In contrast, the Giantin distribution in cell #2 was only minimally affected. The calculated Spearman's rank correlation coefficient of the ratios of cytoplasm/perinuclear area between Giantin and C2GnT-M fluorescence was 0.57 ($P < 0.05$) after BFA treatment for 10 min, 0.68 ($P < 0.01$) for 15 min and 0.62 for 25 min ($P < 0.05$) (Supplementary data, Figure S2). The data indicate that the speed of Golgi disorganization induced by BFA treatment depends on intra-Golgi levels of C2GnT-M.

KD of β-COP results in NMIIA-mediated Golgi fragmentation

Several recent publications show that coat protein complex I (COPI) modulates Golgi organization, and KD of different COPI subunits, especially β-COP, leads to Golgi fragmentation (Guo et al. 2008; Myhill et al. 2008; Wang et al. 2010). It is known that BFA treatment prevents the binding of COPI to the Golgi by suppressing the activation of ADP ribosylation factor (ARF) 1 in the ARF1-GDP exchange factor (GEF)–COPI complex through the inhibition of GEF (Klausner et al. 1992; Lippincott-Schwartz 1993; Stamnes and Rothman 1993; Deng et al. 2009). These observations raised the possibility that NMIIA and glycosyltransferases are involved in morphological changes of the Golgi in cells lacking β-COP. We found that KD of β-COP converted the majority of cells with the normal Golgi morphology, which exhibits structure clustered together in a juxtanuclear array, to cells with altered the Golgi morphology, including condensed, enlarged and fragmented structures (Figure 3A and B). We then proceeded to examine the effect of different β-COP siRNA treatment times, including 48, 60 and 72 h, on the Golgi morphology. After 48 h treatment, the level of β-COP was reduced by up to 50%. In 57.6% of these cells, the Golgi appeared condensed; in 15.5% of the cells, the Golgi was enlarged; and in 6.2% of the cells, the Golgi was fragmented (Figure 3A, B and E). After 60 h treatment with β-COP siRNA, 90% of β-COP was knocked down. The percentage of cells which exhibited condensed Golgi was 28.4%; enlarged Golgi, 41.2%; and fragmented Golgi, 17%. After 72 h treatment with β-COP siRNA, 95% of β-COP was knocked down, and 5.1% of cells had condensed, 20.2% enlarged and 71.2% fragmented Golgi (Figure 3A, B and E). Interestingly, we found that after 60 h treatment with this siRNA, NMIIA was elevated while C2GnT-M was substantially reduced (Figure 3G). Further, the complexes formed between C2GnT-M and NMIIA, and the amounts of ubiquitinated C2GnT-M were increased (Figure 3H). Golgi fragmentation induced by β-COP KD was dependent on NMIIA, demonstrated by loss of the effect after KD of NMIIA. Golgi morphology and C2GnT-M fluorescence intensity in cells treated with a combination of 200 nM β-COP siRNA and 250 nM NMIIA siRNA were indistinguishable from those of the control cells (Figure 3A, C and D). The data indicate that the degree of Golgi fragmentation reflects the extent of β-COP KD.

To validate these observations, we monitored NMIIA and C2GnT-M colocalization in cells treated for 60 h with β-COP siRNA. In these cells, we detected an increase in C2GnT-M and NMIIA complexes and the Golgi enlargement was accompanied by increased C2GnT-M and NMIIA Mander's overlap coefficient. In both control and β-COP KD cells, the colocalization of these proteins was detected at the periphery of the Golgi (Petrosyan, Ali, Verma, et al. 2012), and in β-COP KD-cells, the NMIIA and C2GnT-M colocalization area was more extensive as the Golgi expanded (Figure S3). Taken together, the data lend further support of the involvement of the NMIIA and Golgi residential protein (C2GnT-M) in the β-COP KD-induced Golgi fragmentation.

Heat shock protein inhibitor, KNK437, arrests C2GnT-M in the ER and causes a delay of the BFA-induced Golgi collapse in Panc1-bC2GnT-M (c-Myc) cells

Recently, we found that several isoforms of HSP70 (heat shock protein 70), including heat shock 70 kDa protein 8

fluorescence intensity of Giantin in cytoplasm vs Golgi (perinuclear area) was analyzed and plotted against times of BFA treatment. After treatment for 10 min, cytoplasmic Giantin staining in (WT)C2GnT-M cDNA-treated cells was increased from 22 to 50%, while only 9% increase was observed in mutant C2GnT-M cDNA-treated cells; *$P < 0.001$ for C2GnT-M (A^4AA^6)-GFP vs C2GnT-M (WT)-GFP. The bars at 0 min represent the fluorescence intensity of C2GnT-M in untreated cells. (**F**) Determination of the distribution of fluorescence signal in the perinuclear area (Golgi) and cytoplasm as described in the *Materials and methods* section. (**G**) Confocal immunofluorescence images of bC2GnT-M and Giantin in Panc1-bC2GnT-M (c-Myc) cells treated with BFA for up to 25 min. The fluorescence intensity distribution of Giantin (cytoplasm vs perinuclear area) and C2GnT-M total fluorescence were analyzed in 60 cells at each time point after BFA treatment for 10, 15 or 25 min. Representative cells with high and low expression of bC2GnT-M presented on the right hand side (zoomed C2GnT-M and Giantin). The cells with higher expression of C2GnT-M (1, 3 and 5) demonstrate higher sensitivity to BFA treatment than cells with lower expression of C2GnT-M (2, 4 and 6, respectively). (**H**) Quantification of the cytoplasm/perinuclear area ratio of Giantin fluorescence at different time points of BFA treatment in cells with low (up to 30 000 a.u.) and high (over 30 000 a.u.) C2GnT-M integrated fluorescence. The bars at 0 min represent data obtained from untreated cells; *$P < 0.001$. The results shown are from three independent experiments. All confocal images were acquired with the same imaging parameters; bars, 10 μm.

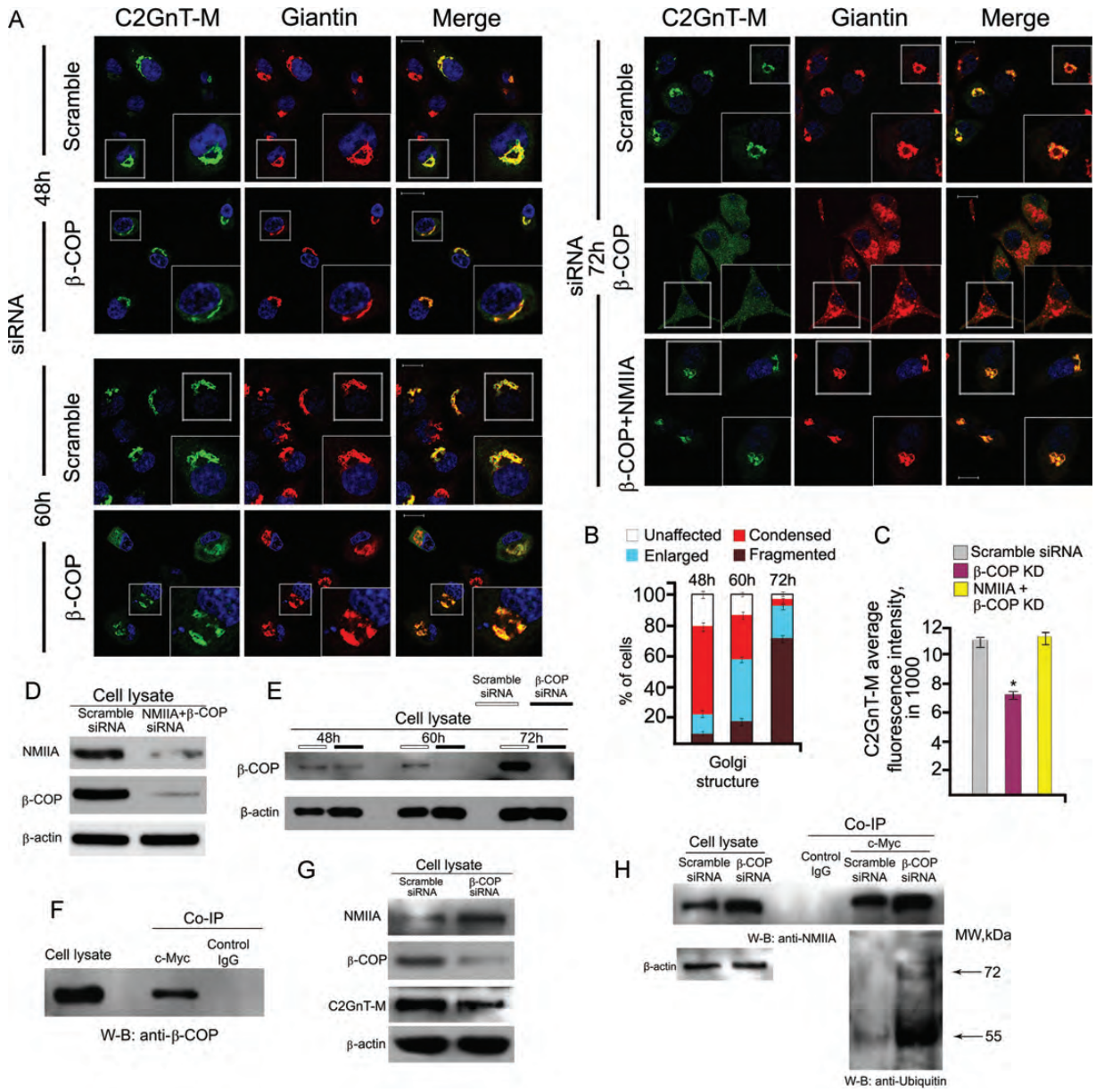

Fig. 3. NMIIA and C2GnT-M are involved in Golgi fragmentation after KD of β-COP in Panc1-bC2GnT-M (c-Myc) cells. (**A**) Confocal immunofluorescence images of bC2GnT-M and Giantin in cells ($n = 30$ for every group of cells) treated with scramble siRNA or β-COP siRNA for 48, 60 and 72 h and mixture of β-COP and NMIIA siRNAs for 72 h. White boxes of the images indicate representative cells enlarged in the inset. (**B**) Quantification of a different Golgi phenotype in cells treated with β-COP siRNA for 48, 60 and 72 h. (**C**) Quantification of bC2GnT-M fluorescence intensity in cells treated with scramble, β-COP or β-COP + NMIIA siRNAs. β-COP KD resulted in Golgi expansion and fragmentation, accompanied by bC2GnT-M degradation, which were prevented by KD of NMIIA. *$P < 0.001$ for β-COP siRNA vs scramble siRNA or NMIIA + β-COP siRNAs. (**D**) NMIIA and β-COP western blots of the lysates of cells treated with scramble or mixture of β-COP and NMIIA siRNAs. (**E**) β-COP western blot of the lysates of cells treated with scramble or β-COP siRNAs for different time points. (**F**) β-COP western blot of the complexes pulled down with anti-c-Myc Abs from the lysates of control cells. bC2GnT-M forms complex with β-COP. (**G**) NMIIA, β-COP and c-Myc western blots of the lysates of cells treated with scramble or β-COP siRNAs for 60 h. β-COP KD increased NMIIA but decreased C2GnT-M. (**H**) NMIIA and Ubiquitin western blots of the complexes pulled down with anti-c-Myc Abs from the lysates of cells treated with β-COP siRNA for 60 h. β-COP KD increased the formation of NMIIA-bC2GnT-M complexes. Equal amounts of proteins in the lysates were used for Co-IP, and β-actin was used as a loading control. The results shown are representative of three independent experiments. All confocal images were acquired with the same imaging parameters; bars, 10 μm.

(HSP70-8), are involved in the Golgi targeting of C2GnT-M (Petrosyan, Ali, Verma, et al. 2012) in Panc1-bC2GnT-M (c-Myc) cells. Treatment of these cells with 50 μM KNK437, a HSP inhibitor (Yokota et al. 2000) for 1 h shifted the distribution of C2GnT-M from Golgi to ER in an NMIIA-dependent manner while the Golgi architecture was unaltered (Petrosyan, Ali, Verma, et al. 2012). We reasoned that the depletion of Golgi C2GnT-M by the inhibition of HSPs would

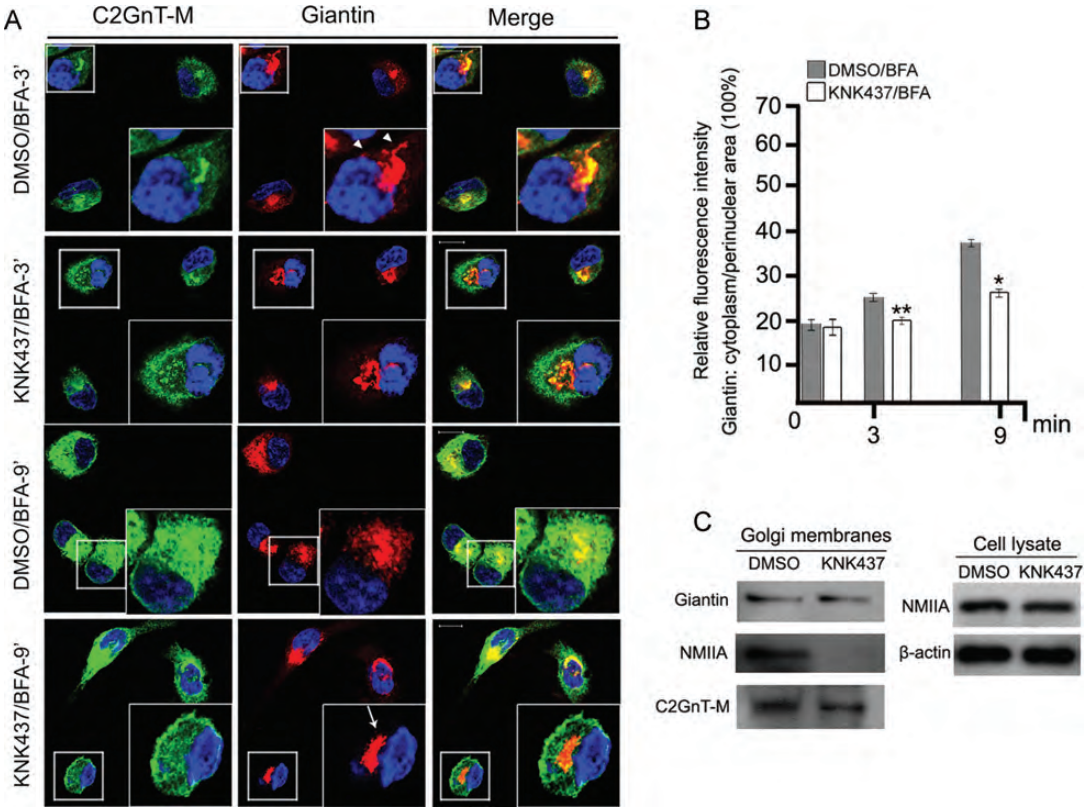

Fig. 4. HSP inhibition decreases C2GnT-M and NMIIA in the Golgi and therefore reduces response to BFA. (**A**) Confocal immunofluorescence images of bC2GnT-M and Giantin in Panc1-bC2GnT-M (c-Myc) cells ($n = 60$) treated with DMSO or KNK437 followed by treatment with BFA for 3 and 9 min (DMSO/BFA-3′(9′); KNK437/BFA-3′(9′)). In DMSO/BFA-3′-treated cells, Golgi extended by tubular elements (white arrowheads); similar structures but only after 9 min (white arrow) found in KNK/BFA-9′-treated cells. White boxes of the images indicate representative cells enlarged in the inset. (**B**) Quantification of Giantin fluorescence cytoplasm/perinuclear area in cells described in (A). $^{**}P < 0.01$; $^{*}P < 0.001$ for KNK437/BFA vs DMSO/BFA. The bars at 0 min represent the fluorescence distribution of Giantin in cells pretreated with DMSO or KNK437. (**C**) Golgi membranes were isolated from cells treated with DMSO or KNK437 as described in the *Materials and methods* section and 20 μg of total protein was immunoblotted to detect Giantin, NMIIA and bC2GnT-M. Giantin was used as a loading control. The total cell lysates obtained from cells treated with DMSO or KNK437 were blotted with NMIIA Ab; β-actin was used as a loading control. The results shown are representative of three independent experiments. All confocal images were acquired with the same imaging parameters; bars, 10 μm.

delay the BFA-induced Golgi collapse. Following the treatment of Panc1-bC2GnT-M (c-Myc) cells with dimethyl sulfoxide (DMSO) (control) or 50 μM KNK437 for 1 h, both cells were further treated with 36 μM BFA for 3 and 9 min. In control cells, 3 min treatment with BFA resulted in the appearance of tubular elements extended from the Golgi (Figure 4A, white arrowheads). Meantime, in cells pretreated with KNK437, the bulk of C2GnT-M was found in the ER as a result of the inhibition of the ER-to-Golgi transport of the newly synthesized enzyme due to the inhibition of HSP70 combined with the uninterrupted retrograde transport of the Golgi enzyme to the ER (Petrosyan, Ali, Verma, et al. 2012), while the Golgi architecture remained intact. The 9 min BFA treatment caused a significant change of the Golgi morphology in control cells from well-organized to diffuse structure as monitored by Giantin staining. However, in KNK437-pretreated cells, no apparent morphological changes (white arrow) were observed (Figure 4A and B). The results demonstrate that the absence of C2GnT-M in the Golgi abrogates the BFA-induced Golgi collapse and the Golgi matrix protein Giantin is not involved in this process. To further confirm that the delay of response to BFA is a consequence of reduced presence of NMIIA on the Golgi, we analyzed NMIIA and C2GnT-M in the Golgi membranes isolated from cells treated with DMSO or KNK437. We found a reduced amount of C2GnT-M and greatly depleted NMIIA in the Golgi isolated from KNK437-treated cells when compared with those isolated from DMSO-treated cells. Note that the decrease in NMIIA is Golgi-specific because the total amount of this protein in KNK-treated cells was indistinguishable from that in the control (Figure 4C). These results validate that the BFA-induced Golgi collapse is specific to the Golgi residential (C2GnT-M) and not matrix (Giantin) proteins.

KD of C2GnT-L and ST3Gal1 or treatment with tunicamycin retards BFA-induced Golgi disorganization in LNCaP cells

The model used above to characterize glycosyltransferase-dependent, NMIIA-mediated Golgi fragmentation employs cells that express an epitope-tagged C2GnT-M. To determine if this process is generalizable to other glycosyltransferases, especially in cells expressing endogenous glycosyltransferases, we chose

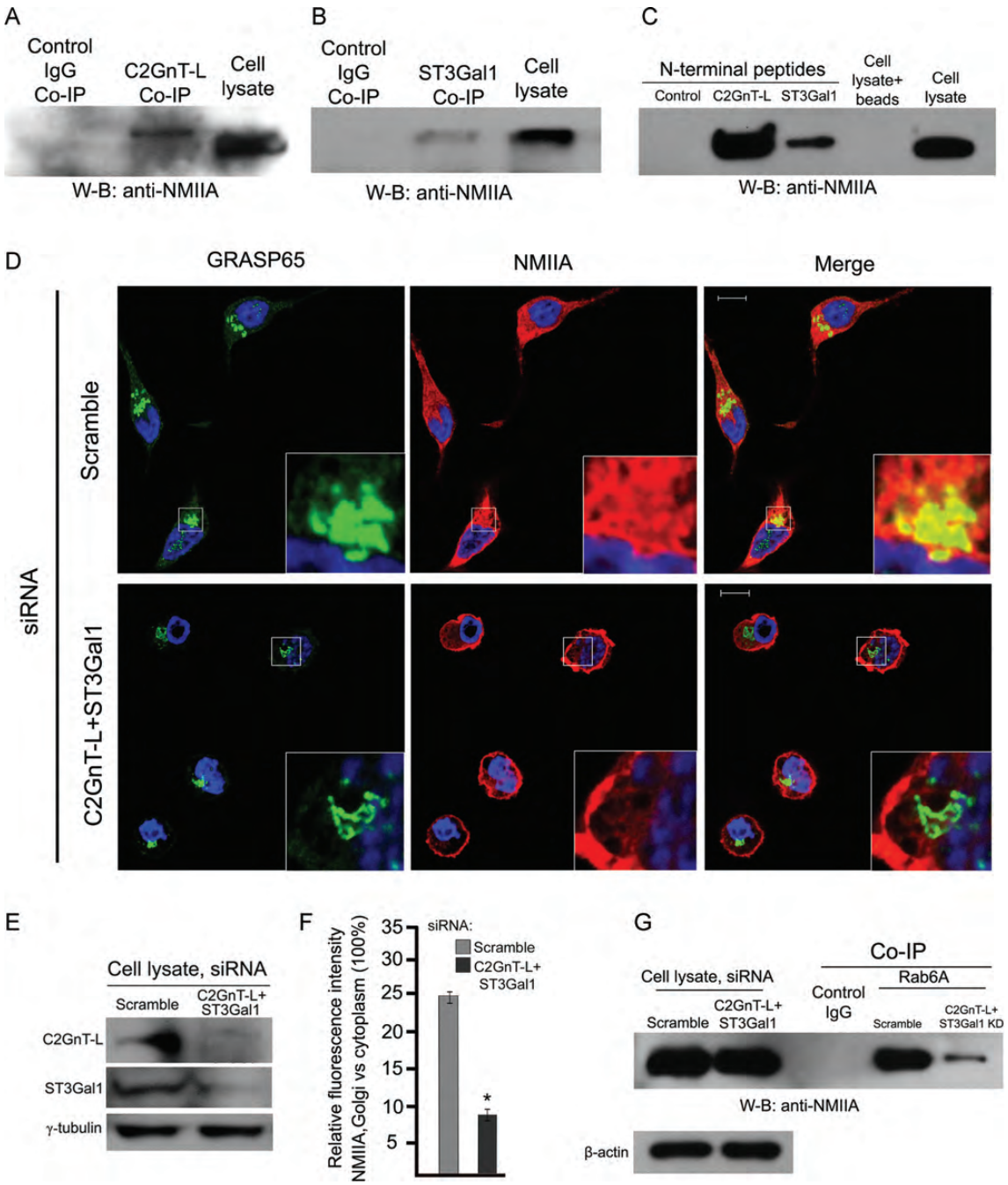

Fig. 5. KD of C2GnT-L and ST3Gal1 abolishes Golgi localization of NMIIA in LNCaP cells. (**A** and **B**) NMIIA western blots of the complexes pulled down with anti-C2GnT-L and ST3Gal1 Abs from the cell lysates. C2GnT-L and ST3Gal1 form complexes with NMIIA. (**C**) NMIIA western blot of the complexes pulled down from cell lysates with biotinylated control peptide, hC2GnT-L and hST3Gal1 N-terminal peptides, cell lysate proteins isolated by magnetic beads without peptides and cell lysate. (**D**) Confocal immunofluorescence images of Golgi marker (GRASP65) and NMIIA in cells ($n = 60$) treated with scramble or C2GnT-L + ST3GAL1 siRNAs. White boxes in the images indicate representative cells enlarged in the inset. (**E**) C2GnT-L and ST3Gal1 western blot of lysate of cells treated with scramble or mixture of ST3GAL1 and GCNT1 (*C2GnT-L*) siRNAs; γ-tubulin was used as a loading control. (**F**) Quantification of NMIIA relative fluorescence intensity Golgi vs cytoplasm in cells presented in (D); $^*P < 0.001$ compared with control. (**G**) NMIIA western blot of the complexes pulled down with the anti-Rab6A Ab from the lysates of cells treated with scramble or C2GnT-L + ST3GAL1 siRNAs. The KD of ST3GAL1 and C2GnT-L reduced the formation of NMIIA-Rab6A complexes. Equal amounts of proteins in the lysates were used for Co-IP, and β-actin was used as a loading control. The results shown are representative of three independent experiments. All confocal images were acquired with the same imaging parameters; bars, 10 μm.

LNCaP cells as the test model. LNCaP cells express high levels of two glycosyltransferases, core 2 *N*-acetylglucosaminyltransferase leukocyte-type (C2GnT-L) and β-galactoside α-2,3sialyltransferase 1 (ST3Gal1), which exhibit ~1.4 and 2.8% of the expression level of glyceraldehyde 3-phosphate dehydrogenase (*GAPDH*), respectively (Gao et al. 2012). C2GnT-L and ST3Gal1 are

localized to *cis/medial*- and *medial/trans*-Golgi, respectively (Whitehouse et al. 1997; Dalziel et al. 2001). NMIIA was pulled down by anti-C2GnT-L or anti-ST3Gal1 Abs (Figure 5A and B) or biotinylated CT of either enzyme (Figure 5C). The results confirmed that both enzymes formed complexes with NMIIA. Interestingly, the amount of NMIIA pulled down by C2GnT-L CT was substantially more than that by ST3Gal1 CT, suggesting a different binding affinity of NMIIA with the CTs of these two enzymes. NMIIA was not pulled down by the control peptide or captured by Dynabeads M-280 Streptavidin.

Next, we examined the intracellular distribution of NMIIA after combined KD of C2GnT-L and ST3Gal1 by treatment with 150 nM C2GnT-L plus 150 nM ST3Gal1 siRNAs for 72 h. NMIIA was detected in the Golgi area identified by GRASP65 staining of the control cells, but its presence in the Golgi was greatly reduced after KD of 90% of C2GnT-L + ST3Gal1, which are referred as LNCaP-KD cells (Figure 5D and E). Quantification of the relative fluorescence intensity of NMIIA at the Golgi vs ER indicated that the fraction of NMIIA that was present on the Golgi surface in control cells was far greater than that in cells lacking C2GnT-L and ST3Gal1 (Figure 5F). The result supports the notion that the NMIIA Golgi localization depends on glycosyltransferases.

To further confirm that NMIIA forms complexes with Golgi glycosyltransferases and Golgi-associated proteins, such as Rab6A, a GTPase known to interact directly with NMIIA (Miserey-Lenkei et al. 2010), we performed series of pulldown experiments using anti-Giantin, anti-GRASP65 or anti-Rab6A Abs. We did not find any association of NMIIA with Giantin or

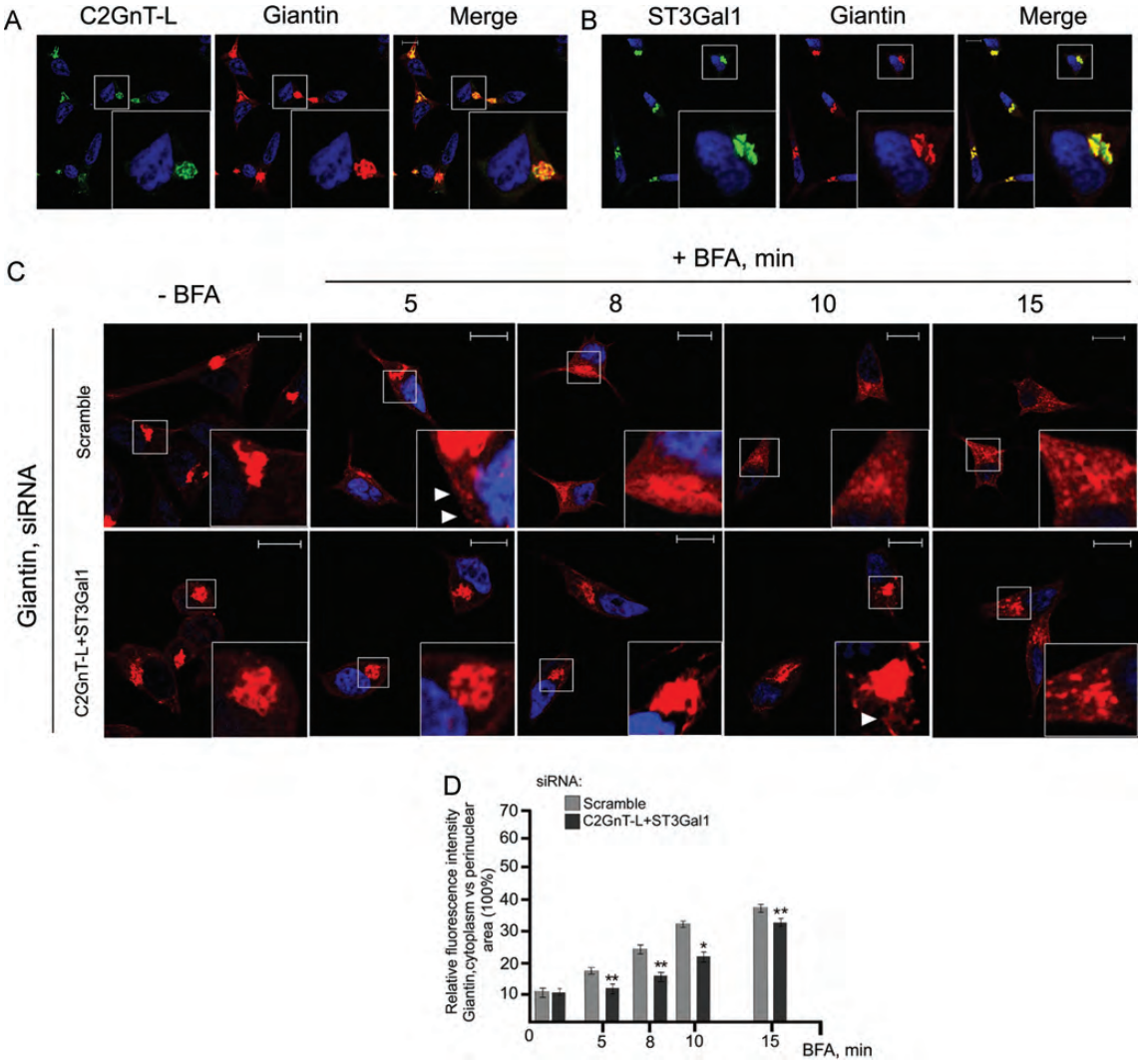

Fig. 6. Combined depletion of C2GnT-L and ST3Gal1 delays BFA-induced Golgi disorganization in LNCaP cells. (**A** and **B**) Confocal immunofluorescence images of C2GnT-L or ST3Gal1 with Giantin. (**C**) Time-dependent changes of the intracellular distribution of Giantin in control and C2GnT-L + ST3Gal1 LNCaP-KD cells treated with BFA for up to 15 min. White boxes in the images indicate Golgi areas enlarged in the inset. The tubules formation in control cells was observed initially at 5 min (arrowheads), while in C2GnT-L + ST3Gal1 LNCaP-KD cells at 10 min. (**D**) Quantification of Giantin relative cytoplasm vs perinuclear area fluorescence intensity in cells shown in (C) ($n = 30$); $^{**}P < 0.01$, $^{*}P < 0.001$ compared with control. The bars at 0 min represent the fluorescence distribution of Giantin in cells pretreated with scramble or C2GnT-L + ST3Gal1 siRNAs. The results shown are the representative of three independent experiments. All confocal images were acquired with the same imaging parameters; bars, 10 μm.

GRASP65 (Figure S4), but a large fraction of NMIIA was detected in the Rab6A immunoprecipitate (Figure 5G). Combined KD of C2GnT-L and ST3Gal1 reduced the NMIIA–Rab6A complex, which is consistent with decreased NMIIA immunofluorescence after KD of these two glycosyltransferases. Together, these results suggest that in LNCaP cells, due to their high expression levels, C2GnT-L and ST3Gal1 are the prime binding targets of NMIIA on the Golgi surface.

To further confirm that NMIIA and glycosyltransferase interactions play a key role in the BFA-induced Golgi fragmentation, we carefully analyzed the Golgi morphology in DMSO- or BFA-treated LNCaP cells. By confocal immunofluorescence microscopy, both C2GnT-L and ST3Gal1 were detected in the Golgi and colocalized with Giantin with minimal signal present in the cytoplasm in control cells (Figure 6A and B). LNCaP-KD cells exhibited a delay in Golgi fragmentation in response to BFA treatment (Figure 6C and D). After only 5 min of BFA treatment (Figure 6C), most of the Giantin in control cells still remained condensed in the juxtanuclear area, while the expansion of the Golgi and the formation of long tubules (white arrowheads) were already detected. In LNCaP-KD cells, similar changes in the Golgi

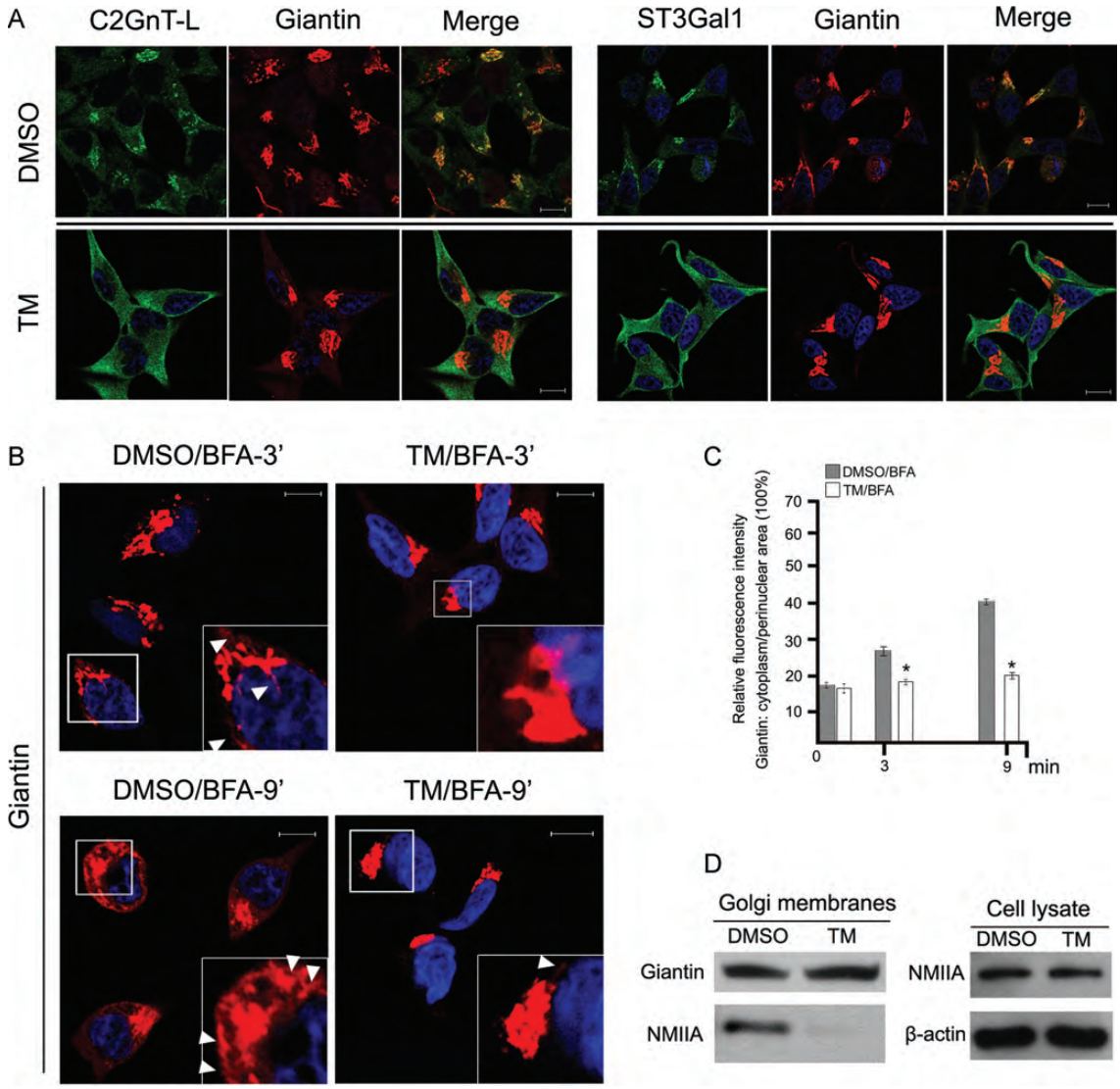

Fig. 7. TM arrests C2GnT-L and ST3Gal1 in the ER and causes the delay of BFA-induced Golgi fragmentation in LNCaP cells. (**A**) Confocal immunofluorescence images of C2GnT-L, ST3Gal1 and Giantin in cells ($n = 60$) treated with DMSO or TM. (**B**) Immunofluorescence images of Giantin in cells treated with DMSO or TM followed by treatment with BFA for 3 and 9 min (DMSO/BFA-3′(9′); TM/BFA-3′(9′)). White boxes of the images indicate representative cells enlarged in the inset. (**C**) Quantification of the Giantin fluorescence cytoplasm/perinuclear area in cells described in (B). The bars at 0 min represent fluorescence distribution of Giantin in cells pretreated with DMSO or TM. *$P < 0.001$ compared with control. (**D**) Western blot analysis of the Golgi membranes isolated from cells treated with DMSO or TM as described in the *Materials and methods* section. Thirty micrograms of total protein was immunoblotted to detect NMIIA. Giantin was used as a loading control. The total lysates obtained from cells treated with DMSO or TM was blotted with NMIIA Ab; β-actin was used as a loading control. The results shown are representative of three independent experiments. All confocal images were acquired with the same imaging parameters; bars, 10 μm.

morphology were not detected until after 8 min of BFA treatment. At this time, the Golgi in control cells already expanded throughout the cell as shown by the increased distribution of Giantin to the cytoplasm (Figure 6D). In control cells, after 10 min of BFA treatment, only a small fraction of Giantin remains condensed and multiple Golgi remnants were detected at the cell periphery. However, only few radially oriented tubules were detected in LNCaP-KD cells at 10 min. After 15 min of BFA treatment, the peripheral fluorescence intensity of Giantin in LNCaP-KD cells was increased but still remained significantly lower than that of the control cells. After 20 min of BFA treatment, this difference no longer existed (data not shown).

We employed another approach to reduce the levels of glycosyltransferases in the Golgi to further prove the dosage effect of glycosyltransferases in the BFA-mediated and NMIIA-dependent Golgi collapse to the ER. Most Golgi glycosyltransferases, including C2GnT-L and ST3Gal1, contain *N*-glycans (El-Battari et al. 2003). One important function of *N*-glycans is to anchor glycoproteins to calnexin/calreticulin in the ER to facilitate protein folding immediately after the transfer of newly synthesized lipid-linked oligosaccharides to the nascent peptide and the generation of monoglucosylated glycans. Inhibition of the *N*-glycan synthesis with inhibitors, such as tunicamycin (TM), which prevents the synthesis of the lipid-linked oligosaccharide (Ishii and Volpe 1987),

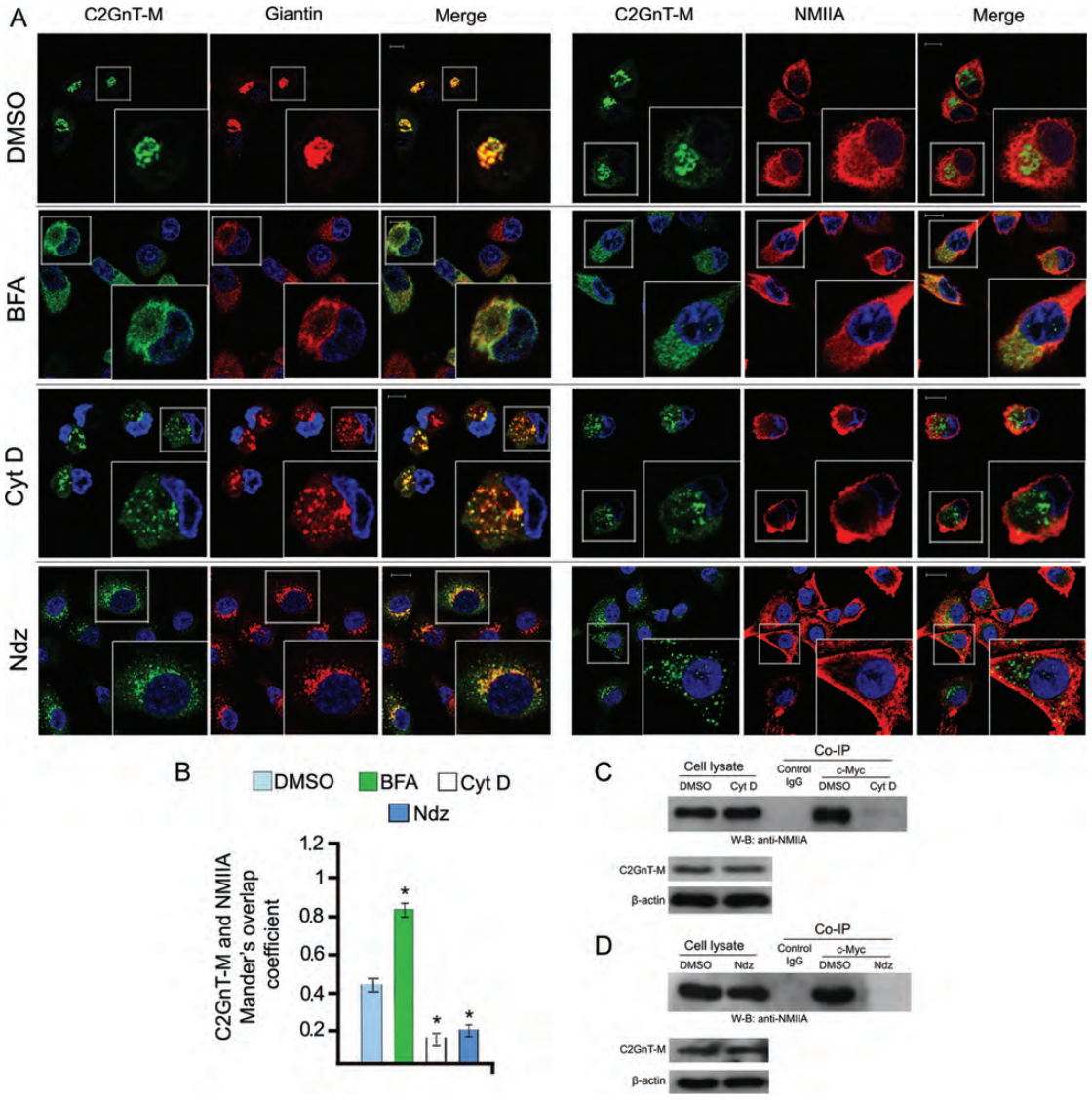

Fig. 8. NMIIA and C2GnT-M are segregated in Cyt D- or Ndz-treated Panc1-bC2GnT-M (c-Myc) cells. (**A**) Confocal immunofluorescence images of C2GnT-M and Giantin or C2GnT-M and NMIIA in cells treated with BFA, Cyt D or Ndz. Representative cells treated with the appropriate amount of DMSO served as a control. White boxes in the images indicate representative cells enlarged in the inset. (**B**) Quantification of Mander's overlap coefficient of C2GnT-M and NMIIA colocalization of cells presented in (A). Data were obtained from 90 cells in three independent experiments. $*P < 0.001$ compared with control. (**C** and **D**) NMIIA western blots of the complexes pulled down with anti-c-Myc Abs from the lysates of cells treated with Cyt D or Ndz. Equal amounts of proteins in the lysates were used for Co-IP. Cyt D or Ndz treatment abolishes the interaction of C2GnT-M with NMIIA. The results shown are representatives of three independent experiments. All confocal images were acquired with the same imaging parameters; bars, 10 μm.

renders these glycoproteins unable to fold properly resulting in their retention in the ER and degradation by proteasomes (Nagai et al. 1997; Prorok-Hamon et al. 2005). Indeed, after 24 h treatment of LNCaP cells with 5 μg/mL of TM, the bulk of C2GnT-L and ST3Gal1 fluorescence staining was detected in the ER (Figure 7A). However, in the DMSO-treated cells, most of the fluorescence signal was found in the Golgi. We proceeded to test whether the TM-induced reduction in Golgi glycosyltransferases would delay the BFA-induced Golgi collapse. DMSO- or TM-treated cells were further exposed to 36 μM BFA for 3 and 9 min and then subjected to analysis of the Giantin distribution by confocal microscopy. Fluorescence analysis and quantification at multiple time points indicated that the fraction of Giantin that appeared in the cytoplasm after BFA treatment in TM-pretreated cells was substantially distinct from the control cells. In the DMSO-treated cells, a significant Golgi expansion with multiple tubular structures was observed after treatment with BFA for 3 min (Figure 7B, white arrowheads). Further, the dissociation of the Golgi along with tubular elements distributed throughout the cell was detected after 9 min treatment with BFA (Figure 7B and C). However, in the TM-treated cells, 3 min treatment with BFA did not cause any significant change in the Golgi morphology. Even after 9 min treatment with BFA, the Golgi still appeared as an intact structure with only single thin tubules extended to the cell periphery (Figure 7B, white arrowhead, and C). The Golgi membranes from cells treated with DMSO or TM for 24 h were isolated and subjected to western blot analysis of NMIIA. As was predicted, the amount of NMIIA in the Golgi of TM-treated cells was substantially reduced (Figure 7D). However, the total amounts of NMIIA in the lysates of TM-treated and control cells were the same. In summary, TM treatment resulted in the ER retention of glycosyltransferases, reduction in Golgi-localized NMIIA and prevention of BFA-induced Golgi fragmentation.

NMIIA-independent Golgi disorganization does not affect the level of C2GnT-M

The Golgi fragmentation induced by BFA treatment or β-COP KD was accompanied by the NMIIA-dependent and proteasome-mediated degradation of C2GnT-M. The results prompted us to ask the question of whether C2GnT-M is degraded under NMIIA-independent Golgi fragmentation conditions. As previously reported (Cole et al. 1996; Rosso et al. 2004), treatment with Cytochalasin D (Cyt D), an actin destabilization agent (May et al. 1998), or nocodazole (Ndz), a microtubule depolymerization agent (Turner and Tartakoff 1989), resulted in extensive Golgi fragmentation (Figure 8A). We found that during Ndz or Cyt D treatment, matrix (Giantin) and non-matrix (C2GnT-M) proteins remained colocalized, indicating that they represented Golgi fragments. While BFA treatment (36 μM for 30 min) causes a complete redistribution of C2GnT-M to the ER where it extensively colocalized with NMIIA, treatment with Cyt D (2 μM for 1 h) or Ndz (40 μM for 30 min) resulted in only minor NMIIA

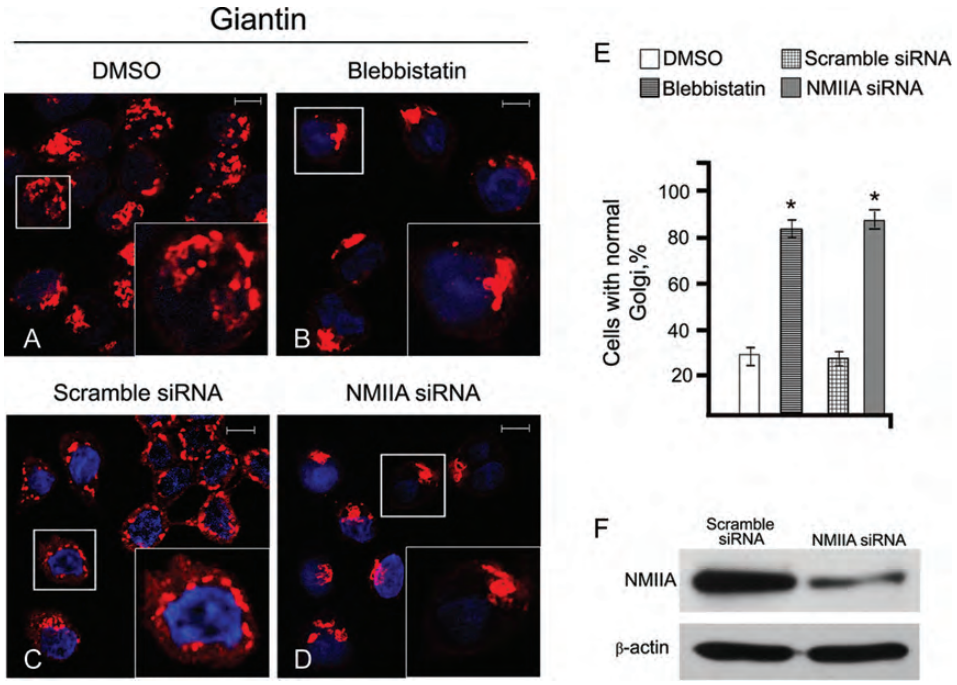

Fig. 9. Inhibition or KD of NMIIA restores the Golgi morphology in HT-29 cells. (**A**–**D**) Confocal immunofluorescence images of Golgi (Giantin) in the cells treated with DMSO, Blebbistatin, scramble or NMIIA siRNA. White boxes in the images indicate representative cells enlarged in the inset. NMIIA inhibition or KD greatly restores normal morphology of the Golgi. (**E**) Percentage of HT-29 cells exhibiting the normal Golgi morphology in cells treated with DMSO or various agents are: DMSO, 30.1%; Blebbistatin, 82.4%; scramble siRNA, 31.8%; NMIIA siRNA, 81.5%; $P < 0.001$ for Blebbistatin vs control and NMIIA siRNA vs scramble siRNA. Patterns of Golgi morphology (Giantin) were analyzed on the complete confocal stacks of 90 cells from three independent experiments. All confocal images were acquired with the same imaging parameters; bars, 10 μm. (**F**) NMIIA western blots of the lysates of HT-29 cells treated with scramble or NMIIA siRNA.

and C2GnT-M colocalization at the cell periphery despite massive Golgi fragmentation (Figure 8B). The result was confirmed by the inability of anti-c-Myc Abs to pulldown NMIIA from the lysates of Panc1-bC2GnT-M (c-Myc) cells treated with either Cyt D or Ndz (Figure 8C and D). Furthermore, the total C2GnT-M fluorescence detected in Ndz- or Cyt D-treated cells was comparable with that of the control cells (Figure 8A, DMSO). Similarly, Cyt D or Ndz treatment had no effect on C2GnT-M levels, measured by immunoblot (Figure 8C and D). We also found that the pretreatment of cells with the NMII inhibitor Blebbistatin did not prevent Cyt D- or Ndz-induced Golgi fragmentation (data not shown). These results indicate that NMIIA-dependent Golgi disorganization involves the proteasome-mediated degradation of ER-targeted Golgi proteins, while NMIIA-independent Golgi fragmentation does not.

Inhibition or KD of NMIIA reverses the Golgi fragmentation in HT-29 cells

HT-29 cells and colon tumor cells have been reported to have fragmented Golgi apparatus (Egea et al. 1993; Kellokumpu et al. 2002). We confirm these reports in HT-29 cells (Figure 9) and stages I–IV colon adenocarcinoma tumor cells by immunohistochemical staining of Giantin (Figure S5). The extensive Golgi fragmentation in HT-29 cells was reversed to a compact morphology after treatment with Blebbistatin or NMIIA siRNA (Figure 9A–F). The percentage of the cells with restored Golgi morphology under various treatment conditions was: DMSO, 30.1%; Blebbistatin, 82.4%; scramble siRNA, 31.8%; NMIIA siRNA, 81.5% (Figure 9E).

Discussion

The Golgi apparatus contains matrix and resident proteins, which are involved in the maintenance of the Golgi architecture and the performance of substrate modification functions, respectively. The steady-state levels of these resident proteins are dynamically regulated by their constant supply provided by the ER-to-Golgi anterograde transport (Petrosyan, Ali and Cheng et al. 2012) and their constant removal for recycling carried out by the Golgi-to-ER retrograde transport (Ward et al. 2001; Petrosyan, Ali, Verma, et al. 2012). In response to stress, the Golgi apparatus undergoes dramatic morphological transformations, ranging from expansion, fragmentation to total dissolution (Siddhanta et al. 2003). Herein, we describe two different mechanisms of these Golgi morphological changes. One is induced by treatment with BFA or KD of β-COP, which results in the accelerated proteasome-mediated degradation of Golgi resident proteins through increased binding NMIIA to these proteins (Figure 10). The other one is induced by microtubule or actin destructive agents, which is NMIIA-independent and does not affect the levels of Golgi resident proteins.

The BFA-induced Golgi collapse is a consequence of inhibition of the ER-to-Golgi anterograde transport (Klausner et al. 1992) coupled with the acceleration of retrograde trafficking. The effect of BFA on the Golgi morphological changes is prevented by the inhibition of NMIIA (Sciaky et al. 1997), although the precise mechanism was not clear (Duran et al. 2003; Vazhappilly et al. 2010). To date, abundant evidence in the literature show that the Golgi-to-ER retrograde transport of Golgi residential proteins is not a COPI-mediated process. For example, the dissociation of COPI from the Golgi membrane does not affect the BFA-induced Golgi disassembly (Scheel et al. 1997). Also, COPI and NMIIA are found on different vesicle populations (Heimann et al. 1999). This finding is supported by a report showing that NMII and Rab6 use COPI-independent vesicles to carry out efficient Golgi-to-ER transport (Miserey-Lenkei et al. 2010). Further, KD of β-COP does not affect the HSP inhibition-induced Golgi-to-ER transport of glycosyltransferases (Petrosyan, Ali, Verma, et al. 2012). Under this condition, NMIIA binds to the Golgi membranes by interacting directly and specifically with the CTs of Golgi resident proteins, such as C2GnT-M (Figure 10A and B). The current study extends these observations by showing a correlation of the efficiency of NMIIA-mediated Golgi fragmentation induced by BFA or β-COP siRNA treatment with the levels of glycosyltransferases in the Golgi. Our results and proposed model provide a rational explanation of how NMIIA is involved in the COPI inhibition-induced fragmentation of the Golgi (Figure 10C).

A growing body of research indicates that at the Golgi, NMIIA tightly interacts with GTPases, such as Rab6A and Rho (Even-Ram et al. 2007; Miserey-Lenkei et al. 2010). Further, myosin II heavy chain binds multiple DbI family GEFs and suppresses its activity, which is accompanied by an increase in myosin II ATPase activity, phosphorylation of light chains and actomyosin assembly (Lee et al. 2010). The data are in good agreement with our observation that BFA-induced GEF inhibition increases NMIIA expression and formation of the complex between NMIIA and glycosyltransferases. This interaction provides a mechanism for anchoring the motor protein, NMIIA, to the Golgi, and moving Golgi membranes to the ER. The movement is aborted when the complex is dissociated following inhibition or KD of NMIIA. We have found that NMIIA interacts with not only C2GnT-M, C2GnT-L and ST3Gal1 but also several other glycosyltransferases (unpublished observation). These data suggest that NMIIA is a universal motor partner of Golgi residential enzymes and its interactions with these enzymes are responsible for Golgi remodeling under basal conditions and Golgi fragmentation under stress.

We have documented in Panc1-bC2GnT-M (c-Myc) cells a direct correlation between intra-Golgi concentrations of ectopically expressed glycosyltransferases and the kinetics of BFA-induced Golgi disorganization: the cells with the low level of C2GnT-M in the Golgi are more resistant to BFA than those with the high level of intra-Golgi C2GnT-M. Similarly, the Golgi in HEK293 cells which express wild-type C2GnT-M-GFP are more sensitive to BFA than cells lacking C2GnT-M-GFP. Our data also show that the glycosyltransferase-mediated Golgi fragmentation is not limited to exogenous enzymes because a reduction in the levels of two endogenous Golgi glycosyltransferases in LNCaP cells also significantly reduces the presence of NMIIA in the Golgi, which results in a delay of BFA-induced Golgi fragmentation. We conclude that glycosyltransferases are the strategic partners of NMIIA at the Golgi. Remarkably, the arrest of C2GnT-M in the ER

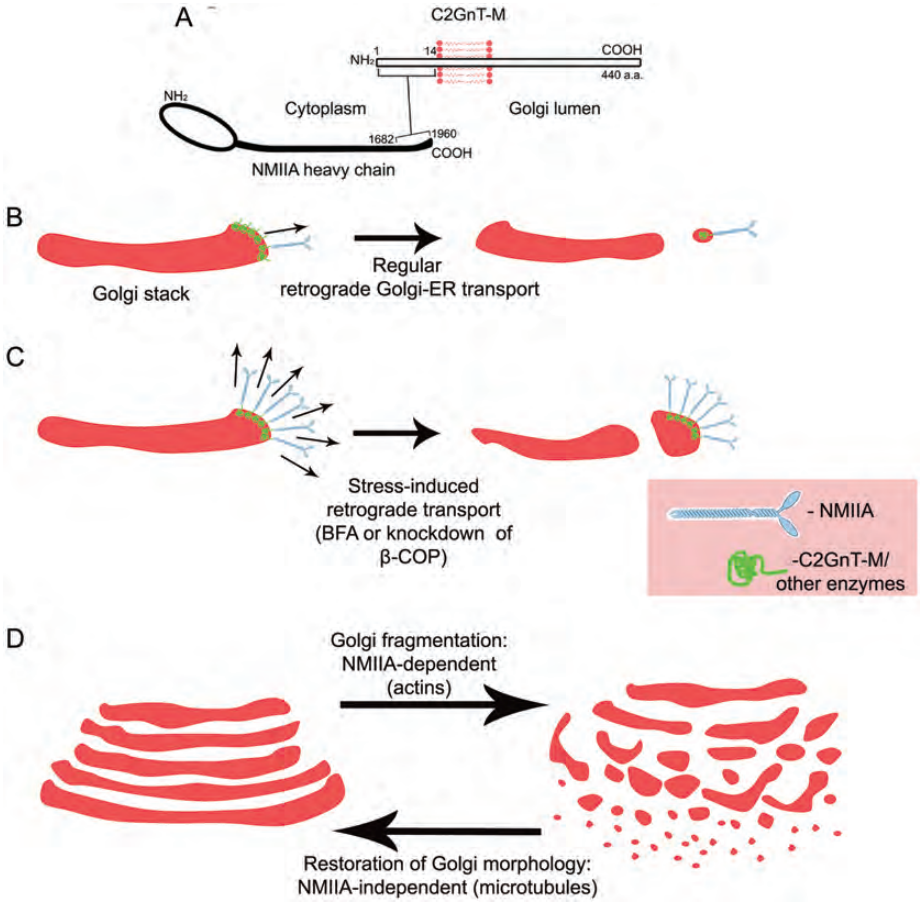

Fig. 10. The proposed model of the Golgi fragmentation mediated by the interaction of NMIIA with glycosyltransferases. (**A**) The diagram showing the interaction of the CT of C2GnT-M with the C-terminal region (1682–1960 amino acids) of the NMIIA heavy chain (Petrosyan, Ali, Verma, et al. 2012). (**B**) Under basal condition, C2GnT-M is bound and removed from the Golgi apparatus by NMIIA as depicted in (A) and transported to the ER for recycling. (**C**) Stress inducers, such as BFA and β-COP siRNA, caused Golgi fragmentation by increasing binding of NMIIA with Golgi proteins such as C2GnT-M. (**D**) The restoration of the Golgi morphology after stress-induced fragmentation requires microtubules and depends on dyneins, HSPs etc., but not NMIIA and actins. NMIIA works in Golgi-ER direction to transport the enzyme to the ER for recycle.

following a brief inhibition of HSP70 (Petrosyan, Ali, Verma, et al. 2012) also leads to an identical outcome. However, the effect of KNK437 treatment is more potent than a simple reduction in C2GnT-M in the Golgi because HSP70 is involved in the folding of many glycosyltransferases other than C2GnT-M (Caramelo et al. 2004; Niimura et al. 2010). Similarly, LNCaP cells treated with TM followed by BFA also retards the BFA-induced Golgi collapse. This effect is more pronounced in TM-treated cells when compared with cells in which C2GnT-L + ST3Gal1 have been knocked down because they represent only two of the many glycosyltransferases affected by TM treatment. Taken together, our results show that the interaction of NMIIA with Golgi glycosyltransferases is required for BFA-induced Golgi disorganization and the sensitivity of the response is correlated with the levels of the glycosyltransferases in the Golgi.

Formation of COPI vesicles is initiated by ARF1 binding to the Golgi membrane followed by the recruitment of additional components and the loading of the cargo before budding from the Golgi (Palmer et al. 1993). Because BFA induces the Golgi collapse by inhibiting COPI binding to the Golgi, we expect to see a similar outcome after siRNA KD of β-COP, a component of COPI vesicles. In cells treated with β-COP siRNA, we have found condensed, enlarged and fragmented Golgi, and the relative abundance of these three different forms of the Golgi morphology varies according to the duration of β-COP siRNA treatment. The condensed Golgi predominates the early phase of the treatment, which is followed by enlarged and then fragmented Golgi as the treatment time is extended. Under normal conditions, β-COP and C2GnT-M form complexes (Figure 3F), and we believe that the condensed Golgi is generated by the disassembly of COPI vesicles involved in the intra-Golgi transport (Waters et al. 1991; Cosson et al. 2002), which occurs early. After that, the pull engineered by the interaction of NMIIA with glycosyltransferases results in expansion and then the fragmentation of the Golgi. It should be mentioned that the NMIIA level is increased and C2GnT-M is reduced following BFA treatment or β-COP KD. Whether the increase in NMIIA is the result of increased gene expression or protein stability remains to be established. The increase in NMIIA was accompanied by elevated NMIIA–glycosyltransferase complexes, which provides sufficient strength to fragment the Golgi. The effect of β-COP KD coupled with BFA treatment requires the interaction of

NMIIA with Golgi glycosyltransferases because inhibition or KD of NMIIA abolishes Golgi fragmentation. Therefore, KD of β-COP results in Golgi disorganization similar to that produced by BFA treatment, although it takes longer for β-COP KD to reach a similar extent of Golgi fragmentation.

Current data also show that Golgi fragmentation can occur in an NMIIA-independent fashion. This phenomenon can be induced by Cyt D or Ndz through the disruption of actins or microtubules, respectively. Destruction of these cytoskeletal structures shuts down anterograde or retrograde vesicular transports, which leads to the destabilization of the Golgi structure. Further, under these conditions, Golgi resident proteins and NMIIA do not colocalize. In both cases, the failure of NMIIA to interact with Golgi resident proteins prevents these proteins from being delivered to the proteasome for degradation (Straight et al. 2003).

NMIIA has been implicated in the Golgi morphological changes associated with apoptosis (Kato et al. 2005). Apoptosis is accompanied by the caspases-mediated cleavage of Golgi matrix proteins, followed by Golgi disassembly, a morphological change similar to mitotic fragmentation (Hicks and Machamer 2005). Interestingly, Golgi fragmentation during apoptosis is independent of major changes in actin and tubulin cytoskeleton, which supports the idea that Golgi fragmentation requires intact actin cables to facilitate the disassembly of this organelle (Mukherjee et al. 2007).

Our recent preliminary observations show that Golgi matrix proteins but not glycosyltransferases are involved in the Golgi reassembly after BFA washout. Rebuilding of the Golgi structure requires HSPs and not NMIIA (manuscript in preparation). The data are in good agreement with the observations that microtubules rather than actin microfilaments are required for the restoration of the Golgi complex or for the ER-to-Golgi anterograde transport (Valderrama et al. 2001). Taken together, our results confirm that NMIIA is involved in Golgi-to-ER but not ER-to-Golgi trafficking (Figure 10B–D). Further, the data lead us to propose that the fragmentation of the Golgi is resulted from the perturbation of Golgi resident proteins which participate in the maintenance of the Golgi morphology. Indeed, it has been reported that Golgi appears as a disassembled structure when glycosyltransferases fail to localize to the Golgi (Quintero et al. 2008; Gill et al. 2010; Pokrovskaya et al. 2011). However, this possibility may be limited only to glycosyltransferases which form complexes with cytoskeletal proteins (Yamaguchi and Fukuda 1995; Wassler et al. 2001).

The Golgi morphological changes as described herein also occur in cancer cell lines such as colon carcinoma HT-29 cells as well as cancer cells in human colon tumors (Egea et al. 1993; Kellokumpu et al. 2002). Interestingly, we are able to restore the Golgi morphology in HT-29 cells by inhibiting NMIIA, implicating NMIIA in causing Golgi fragmentation in these adenocarcinoma cells. However, the contribution of major glycosyltransferases to the formation of this Golgi phenotype remains to be uncovered. Cellular neoplastic transformation is commonly associated with altered glycosylation (Petrosyan and Britan 2006; Petrosyan and Kharchenko 2006; Kubyshkin 2011). Given the role the Golgi apparatus plays in supporting the post-translational modification of secreted and membrane proteins and the reported alteration of Golgi morphology and glycosylation in cancer cells, the elucidation of the mechanism of Golgi fragmentation in cancer cells should help understand the role of this organelle in carcinogenesis.

Materials and methods

Materials

The reagents were obtained from the following suppliers: BFA, KNK437 and MG-132, EMD Chemicals (Brookfield, WI); Blebbistatin, Ndz, Cyt D, TM, mouse monoclonal anti-β-actin and rabbit polyclonal Abs against heavy chain (the peptide GKADGAEAKPAE located at the C terminus of NMIIA), Sigma (St Louis, MO); c-Myc (mouse monoclonal and rabbit polyclonal), mouse monoclonal anti-GRASP65 and γ-tubulin (goat polyclonal) Abs, Santa Cruz Biotechnology (Santa Cruz, CA); anti-human C2GnT-M goat and rabbit polyclonal Abs, Everest Biotech (Oxfordshire, UK) and Aviva Systems Biology (San Diego, CA), respectively; rabbit polyclonal Abs (anti-Giantin, anti-PDI, anti-Ubiquitin), mouse monoclonal anti-β-COP and anti-Rab6A Abs, Abcam (Cambridge, MA); mouse polyclonal Abs anti-C2GnT-L and anti-ST3Gal1, Abnova (Taipei, Taiwan). The horseradish peroxidase (HRP)-conjugated secondary Abs (donkey anti-rabbit, donkey anti-mouse and donkey anti-goat) were obtained from Jackson ImmunoResearch (West Grove, PA). Normal human colon and colon carcinoma tissue arrays were purchased from US Biomax (Rockville, MD).

Cell culture and drug treatment

Panc1-bC2GnT-M (c-Myc) cells were prepared as described previously (Choi et al. 2005). Panc1-bC2GnT-M (c-Myc), HEK293, LNCaP and HT-29 cells were grown at 37°C under 5% CO_2 and water saturated environment in minimum essential medium with Earle's balanced salts (MEM/EBSS) medium, Dulbecco's modified Eagle medium (DMEM), Roswell Park Memorial Institute medium (RPMI) and McCoy's 5A with 1.5 mM L-glutamine (Thermo Fisher Scientific, Inc., Waltham, MA) supplemented with 10% fetal bovine serum and antibiotics (50 U/mL penicillin and 50 μg/mL streptomycin), respectively. Blebbistatin, TM, KNK437, Ndz, Cyt D, BFA and MG-132 were dissolved in dimethyl DMSO immediately before use. Cells treated with a corresponding concentration of DMSO served as controls. BFA was added to the culture cells at a final concentration of 36 μM, which was followed by incubation at 37°C for the times given in each experiment. The next series of experiments were designed to determine the effect of BFA after proteasome inhibition by MG-132. Panc1-bC2GnT-M (c-Myc) cells were treated with 5 μM MG-132 at 37°C for 3 h or for 2 h followed by 36 μM BFA at 37°C for 1 h. Working concentrations of Blebbistatin, TM, KNK437, Ndz and Cyt D for Panc1-bC2GnT-M (c-Myc) cells were 35 μM, 5 μg/mL, 50 μM, 40 μM and 2 μM, respectively; the HT-29 cells have been treated with 70 μM of Blebbistatin.

Co-IP and transfection

For identification of proteins in the complexes pulled down by Co-IP, confluent cells grown in a T75 flask were washed

three times with 6 mL PBS each, harvested by trypsinization and neutralized with the soybean trypsin inhibitor at a 2× weight of trypsin. After washing three times with PBS, the cells were lysed with 1.5 mL of a non-denaturing lysis buffer, which contained 50 mM Tris (pH 7.4), 150 mM NaCl, 5 mM ethylenediamminetetraacetate (EDTA), 0.5% NP-40 (w/w) and 1% (v/v) of mammalian protease inhibitor cocktail (Sigma). One milliliter of cell lysate was precleared by treatment with 50 µL of irrelevant Ab (1 mg/mL) of same species and isotype as that to be employed for IP for 1 h at 4°C. It was followed by incubation with 100 µL of a 50% slurry of protein G plus Agarose (EMD) at 4°C for 1 h with gentle rocking. After centrifugation, an aliquot of the supernatant was incubated with appropriate Abs (1.5 µg Abs to 400 µg protein in 1 mL cell lysate) overnight at 4°C with gentle rocking. Then, 50 µL of protein G agarose slurry was added and incubated for 1 h at 4°C with gentle rocking to capture the immunocomplexes. The pellet was resuspended in lysis buffer and washed with PBS three times. The last pellet was resuspended in sodium dodecyl sulfate (SDS) sample buffer. MYH9 (NMIIA, myosin, heavy polypeptide 9, non-muscle), MYH10 (NMIIB, myosin, heavy polypeptide 10, non-muscle) and scrambled on-target plus smartpool siRNA were purchased from Dharmacon (Chicago, IL). Pool of three siRNA-targeting COPB (β-COP), ST3GAL1 and GCNT1 (C2GnT-L) were obtained from Santa Cruz Biotechnology. Panc1-bC2GnT-M (c-Myc), LNCaP and HT-29 cells were transfected with 100–200 nM siRNAs using Lipofectamine RNAi (Invitrogen, Carlsbad, CA) MAX reagent and media without antibiotics according to the manufacturer's recommendation. After cultured for 72 h, cells were analyzed by western blotting.

Proteins were separated on sodium dodecyl sulfate polyacrylamide gel electrophoresis (SDS–PAGE) on mini-gels with various % gel specified for each experiment (Bio-Rad, Hercules, CA). Western blots were developed using HRP-coupled antibodies, Thermo Scientific SuperSignal West Pico Chemiluminescent Substrate reagents and exposed to BioExpress Blue Basic Autorad chemiluminescence film (Kaysville, UT). The bands on the autoradiography films were digitized by scanning with ScanJet 6200C (Hewlett Packard) driven by Adobe Photoshop.

Plasmid construction and transient transfection in HEK293 cells

The wild-type and mutant hC2GnT-M cDNAs were cloned as described previously (Petrosyan, Ali and Cheng 2012). Transfection of HEK293 cells was carried out using the Lipofectamine 2000 (Invitrogen) following the manufacturer's protocol. After 2–3 days, the transfected cells were used for Co-IP and confocal immunofluorescence microscopy. HEK293 cells were chosen for this experiment because of its high capability for expressing recombinant proteins.

Confocal immunofluorescence microscopy

Panc1-bC2GnT-M (c-Myc), HEK293, LNCaP and HT-29 cells were grown overnight on cover slips placed in a 6-well plate, washed twice with PBS and immediately fixed with 4% paraformaldehyde/PBS for 30 min at room temperature (RT). Then, the fixed cells were incubated with anti-c-Myc, anti-Giantin and anti-NMIIA Abs (1:100); LNCaP cell were stained by anti-GRASP65 (1:200), anti-NMIIA, anti-C2GnT-L (1:100) and anti-ST3Gal1 (1:150) Abs; HEK293 cells were incubated with mouse anti-GFP and rabbit anti-Giantin Abs (1:200, Abcam); HT-29 cells were incubated with rabbit anti-Giantin (1:300). After incubation with primary Abs at 37°C for 1 h followed by washing with phosphate buffered saline + Tween 20 (PBST) three times, cells were stained with DyLight 488-conjugated donkey anti-mouse Ab (green) or DyLight 488-donkey anti-goat Ab (green) and DyLight 594-donkey anti-rabbit Ab (red) (1:200) (Jackson ImmunoResearch). After the final wash in PBST, cells were mounted in the ProLong Gold antifade reagent with or without 4′,6-diamidino-2-phenylindole (DAPI) (Invitrogen). After deparaffinization, normal human colon and colon carcinoma tissue sections were rinsed with water and then treated with 10 mM Tris–1 mM EDTA–0.05% Tween 20 at pH 9 for 20 min in a microwave for 20 min to retrieve the antigen. Following blocking with 1% donkey serum for 1 h at RT, the sections were incubated with anti-C2GnT-M goat polyclonal (1:50) and rabbit polyclonal anti-Giantin Abs (1:150) for 1 h at RT, followed by treatment for 1 h at RT with DyLight 488-conjugated donkey anti-goat Abs (green) and DyLight 594 donkey anti-rabbit secondary Abs (red) (1:200). The treated tissue sections were mounted in the ProLong Gold antifade reagent containing DAPI. Stained cells/tissue sections were examined under a Zeiss 510 Meta Confocal Laser Scanning Microscope performed at the Confocal Microscopy Core Facility of the University of Nebraska Medical Center. Fluorescence was detected using an emission filter of a 505–550 nm band pass for green and a 575–615 nm band pass for red. Images were analyzed using Zeiss 510 software. For some figures, image analysis was performed using the Adobe Photoshop and the ImageJ. The average fluorescence intensity was measured as a mean ± SEM of integrated fluorescence intensity (in arbitrary units, a.u.) or total fluorescence intensity (in pixels) measured for every cell individually. The colocalized points of green and red were determined by Image J plugin "Colocalization" which generate an image of colocalized pixels and superimposed on an RGB-merge of two 8-bit images. Statistical analysis of colocalization was performed by ImageJ calculating the Mander's overlap coefficient, corresponding to the fraction of green pixels that overlap with red pixels in relation to the total green pixels (Comeau et al. 2006). The Golgi region (perinuclear area) and cytoplasm regions were determined using the intensity of the Golgi marker (Giantin or GRASP65) staining. In some cases with diffused Golgi, the whole cell was divided into three areas: nuclear (A), perinuclear (B) and cytoplasmic (C), as schematized by three concentric ellipsoids (Figure 2F). After the subtraction of the nuclear region, the cytoplasm was considered as two-thirds of B + C, while one-third of this sum was denoted as a perinuclear area (Hu and Chien 1997).

Isolation of Golgi membrane fractions by sucrose gradient flotation

Preparation of Golgi membranes performed with the methods described previously (Balch et al. 1984; Mukhopadhyay and Linstedt 2011) with some modifications. Panc1-bC2GnT-M

(c-Myc) and LNCaP cells from ten-twelve 75 cm² cell culture flasks were harvested by PBS containing 0.5× protease inhibitors (1.2 mL per flask). Then, after centrifugation for 5 min at 5000 × g and 4°C, pellet was resuspended in 3 mL of homogenization buffer (0.25 M sucrose, 3 mM imidazole, 1 mM Tris–Cl, pH7.4, 1 mM EDTA). The cells were homogenized by drawing ~30 times through 25-gauge needle until the ratio between unbroken cells and free nuclei becomes 20%:80%. The post-nuclear supernatant was obtained by centrifugation at 600 × g and 4°C for 3 min and then the supernatant was adjusted to 1.4 M sucrose by the addition of ice-cold 2.3 M sucrose containing 10 mM Tris–HCl (pH 7.4). Next, 1.2 mL of 2.3 M sucrose at the bottom of tube was loaded by 1.2 mL of the supernatant followed by sequential overlay by 1.2 mL of 1.2 M and 500 mL of 0.8 M sucrose (10 mM Tris–HCl, pH 7.4). The gradients were centrifuged for 3 h at 100 000 × g (4°C) in SW40 rotor (Beckman Coulter). The turbid band at the 0.8 M/1.2 M sucrose interface containing Golgi membranes was harvested in ~500 mL by the syringe puncture. The fraction at the concentration of ~1.2–1.4 mg protein/mL was used for the experiments mentioned in the *Results* section.

Isolation of NMIIA in LNCaP cell lysates with biotinylated N-terminal peptides of hC2GnT-L or hST3Gal1

N-terminal biotinylated peptides representing CTs of glycosyltransferases hC2GnT-L 10 amino acid peptide MLRTLLRRRL and hST3Gal1 14 amino acid peptide AGSMVTLRKRTLKV were obtained from the GenicBio BioTech (Shanghai, China). Control peptide biotin-GHGTGSTGSGSMLRTLLRRRL was purchased from LifeTein LLC (South Plainfield, NJ). To isolate NMIIA, 20 μL of C2GnT-L or ST3Gal1 peptide in 25% acetic acid (0.1 mg/mL) was mixed with 20–40 μL of cell lysate (1.5–3.5 mg/mL of protein). After incubation at 37°C for 1 h, 100 μL of Dynabeads M-280 Streptavidin (Dynal, Norway) was added. Following gentle rotation for additional 30 min, the beads with immobilized complexes were trapped with a magnet. The captured proteins were separated on 8% SDS–PAGE followed by western blotting with anti-NMIIA Abs. The control peptide was used by the same procedure; another sample of the cell lysate incubated with the appropriate amount of 25% acetic acid and followed by treatment with Dynabeads served as a control.

Miscellaneous

Protein concentrations were determined with the Coomassie Plus Protein Assay (Pierce Chemical Co., Rockford, IL) using bovine serum albumin as the standard. Data are expressed as the mean ± SEM. Analysis was performed using the two-sided *t*-test. A value of $P < 0.05$ was considered statistically significant.

Supplementary data

Supplementary data for this article is available online at http://glycob.oxfordjournals.org/.

Funding

This work is supported in part by the Office of Research and Development, Medical Research Service, Department of Veterans Affairs (VA 1I1BX000985), the NIH (1R21HL097238 and 2RO1HL48282) and the State of Nebraska (LB506).

Acknowledgements

We thank Dr Mohamed F. Ali for plasmid construction, Mrs Helen Cheng for excellent technical assistance, Ms Janice A. Taylor at the Confocal microscopy Core Facility for assistance in confocal immunofluorescence microscopy and Dr Justin Mott for critical review of the manuscript.

Conflict of interest

None declared.

Abbreviations

ARF, ADP ribosylation factor; BFA, brefeldin A; C2GnT-L, core 2 *N*-acetylglucosaminyltransferase leukocyte-type; C2GnT-M, core 2 β1,6 *N*-acetylglucosaminyltransferase mucus-type or isozyme 2; Co-IP, coimmunoprecipitation; COPI, coat protein complex I; CT, cytoplasmic tail; Cyt D, Cytochalasin D; GEF, ARF1-GDP exchange factor; HRP, horseradish peroxidase; HSP70, heat shock protein 70; KD, knockdown; Ndz, nocodazole; NMIIA, non-muscle myosin IIA; ST3Gal1, β-galactoside α-2,3-sialyltransferase 1; TM, tunicamycin.

References

Ali MF, Chachadi VB, Petrosyan A, Cheng PW. 2012. Golgi phosphoprotein 3 determines cell binding properties under dynamic flow by controlling Golgi localization of core 2 N-acetylglucosaminyltransferase 1. *J Biol Chem*. 287:39564–39577.

Allan VJ, Thompson HM, McNiven MA. 2002. Motoring around the Golgi. *Nat Cell Biol*. 4:E236– E242.

Balch WE, Dunphy WG, Braell WA, Rothman JE. 1984. Reconstitution of the transport of protein between successive compartments of the Golgi measured by the coupled incorporation of N-acetylglucosamine. *Cell*. 39:405–416.

Bendayan M. 1985. Ultrastructural localization of cytoskeletal proteins in pancreatic secretory cells. *Can J Biochem Cell Biol*. 63:680–690.

Burke J, Pettitt JM, Humphris D, Gleeson PA. 1994. Medial-Golgi retention of N-acetylglucosaminyltransferase I. Contribution from all domains of the enzyme. *J Biol Chem*. 269:12049–12059.

Caramelo JJ, Castro OA, de Prat-Gay G, Parodi AJ. 2004. The endoplasmic reticulum glucosyltransferase recognizes nearly native glycoprotein folding intermediates. *J Biol Chem*. 279:46280–46285.

Cheng P-W, Radhakrishnan P. 2011. Mucin glycan branching enzymes: structure, function and gene regulation. In: Wu A, editor. *Molecular Immunology of Complex Carbohydrates-3. Advances in Experimental Medicine and Biology*, vol. 705. New York: Plenum Press. p. 465–492.

Choi KH, Basma H, Singh J, Cheng PW. 2005. Activation of CMV promoter-controlled glycosyltransferase and beta-galactosidase glycogenes by butyrate, tricostatin A, and 5-aza-2′-deoxycytidine. *Glycoconj J*. 22:63–69.

Cole NB, Sciaky N, Marotta A, Song J, Lippincott-Schwartz J. 1996. Golgi dispersal during microtubule disruption: Regeneration of Golgi stacks at peripheral endoplasmic reticulum exit sites. *Mol Biol Cell*. 7:631–650.

Comeau JW, Costantino S, Wiseman PW. 2006. A guide to accurate fluorescence microscopy colocalization measurements. *Biophys J*. 91:4611–4622.

Conti MA, Adelstein RS. 2008. Nonmuscle myosin II moves in new directions. *J Cell Sci*. 121:11–18.

Cosson P, Amherdt M, Rothman JE, Orci L. 2002. A resident Golgi protein is excluded from peri-Golgi vesicles in NRK cells. *Proc Natl Acad Sci USA*. 99:12831–12834.

Dalziel M, Whitehouse C, McFarlane I, Brockhausen I, Gschmeissner S, Schwientek T, Clausen H, Burchell JM, Taylor-Papadimitriou J. 2001. The relative activities of the C2GnT1 and ST3Gal-I glycosyltransferases

determine O-glycan structure and expression of a tumor-associated epitope on MUC1. *J Biol Chem*. 276:11007–11015.
Deng Y, Golinelli-Cohen MP, Smirnova E, Jackson CL. 2009. A COPI coat subunit interacts directly with an early-Golgi localized Arf exchange factor. *EMBO Rep*. 10:58–64.
DePina AS, Wöllert T, Langford GM. 2007. Membrane associated nonmuscle myosin II functions as a motor for actin-based vesicle transport in clam oocyte extracts. *Cell Motil Cytoskeleton*. 64:739–755.
Dippold HC, Ng MM, Farber-Katz SE, Lee SK, Kerr ML, Peterman MC, Sim R, Wiharto PA, Galbraith KA, Madhavarapu S, et al. 2009. GOLPH3 bridges phosphatidylinositol-4- phosphate and actomyosin to stretch and shape the Golgi to promote budding. *Cell*. 139:337–351.
Durán JM, Valderrama F, Castel S, Magdalena J, Tomás M, Hosoya H, Renau-Piqueras J, Malhotra V, Egea G. 2003. Myosin motors and not actin comets are mediators of the actin-based Golgi-to-endoplasmic reticulum protein transport. *Mol Biol Cell*. 14:445–459.
Dusseljee S, Wubbolts R, Verwoerd D, Tulp A, Janssen H, Calafat J, Neefjes J. 1998. Removal and degradation of the free MHC class II beta chain in the endoplasmic reticulum requires proteasomes and is accelerated by BFA. *J Cell Sci*. 111:2217–2226.
Egea G, Francí C, Gambús G, Lesuffleur T, Zweibaum A, Real FX. 1993. cis-Golgi resident proteins and O-glycans are abnormally compartmentalized in the RER of colon cancer cells. *J Cell Sci*. 105:819–830.
El-Battari A, Prorok M, Angata K, Mathieu S, Zerfaoui M, Ong E, Suzuki M, Lombardo D, Fukuda M. 2003. Different glycosyltransferases are differentially processed for secretion, dimerization, and autoglycosylation. *Glycobiology*. 13:941–953.
Even-Ram S, Doyle AD, Conti MA, Matsumoto K, Adelstein RS, Yamada KM. 2007. Myosin IIA regulates cell motility and actomyosin-microtubule crosstalk. *Nat Cell Biol*. 9:299–309.
Fath KR. 2005. Characterization of myosin-II binding to Golgi stacks in vitro. *Cell Motil Cytoskeleton*. 60:222–235.
Gao Y, Chachadi VB, Cheng PW, Brockhausen I. 2012. Glycosylation potential of human prostate cancer cell lines. *Glycoconj J*. 29:525–537.
Gill DJ, Chia J, Senewiratne J, Bard F. 2010. Regulation of O-glycosylation through Golgi-to-ER relocation of initiation enzymes. *J Cell Biol*. 189:843–858.
Grabenhorst E, Conradt HS. 1999. The cytoplasmic, transmembrane, and stem regions of glycosyltransferases specify their in vivo functional sublocalization and stability in the Golgi. *J Biol Chem*. 274:36107–36116.
Guo Y, Punj V, Sengupta D, Linstedt AD. 2008. Coat-tether interaction in Golgi organization. *Mol Biol Cell*. 19:2830–2843.
Heimann K, Percival JM, Weinberger R, Gunning P, Stow JL. 1999. Specific isoforms of actin-binding proteins on distinct populations of Golgi-derived vesicles. *J Biol Chem*. 274:10743–10750.
Hicks SW, Machamer CE. 2005. Golgi structure in stress sensing and apoptosis. *Biochim Biophys Acta*. 1744:406–414.
Hu YL, Chien S. 1997. Effects of shear stress on protein kinase C distribution in endothelial cells. *J Histochem Cytochem.* 45:237–249.
Ikonen E, de Almeid JB, Fath KR, Burgess DR, Ashman K, Simons K, Stow JL. 1997. Myosin II is associated with Golgi membranes: Identification of p200 as nonmuscle myosin II on Golgi-derived vesicles. *J Cell Sci*. 110:2155–2164.
Ishii S, Volpe JJ. 1987. Dolichol-linked glycoprotein synthesis in G1 is necessary for DNA synthesis in synchronized primary cultures of cerebral glia. *J Neurochem*. 49:1606–1612.
Kato M, Fukuda H, Nonaka T, Imajoh-Ohmi S. 2005. Cleavage of nonmuscle myosin heavy chain-A during apoptosis in human Jurkat T cells. *J Biochem*. 137:157–166.
Kellokumpu S, Sormunen R, Kellokumpu I. 2002. Abnormal glycosylation and altered Golgi structure in colorectal cancer: dependence on intra-Golgi pH. *FEBS Lett*. 516:217–224.
Klausner RD, Donaldson JG, Lippincott-Schwartz J. 1992. Brefeldin A: Insights into the control of membrane traffic and organelle structure. *J Cell Biol*. 116:1071–1080.
Korn ED, Hammer JA. 1988. Myosins of nonmuscle cells. *Annu Rev Biophys Chem*. 17:23–45.
Kubyshkin AV. 2011. *General and Clinical Pathophysiology.* Vinnytsia, Ukraine: Nova Knyha Publishers.
Lee CS, Choi CK, Shin EY, Schwartz MA, Kim EG. 2010. Myosin II directly binds and inhibits Dbl family guanine nucleotide exchange factors: A possible link to Rho family GTPases. *J Cell Biol*. 190:663–674.
Lippincott-Schwartz J. 1993. Membrane cycling between the ER and Golgi apparatus and its role in biosynthetic transport. *Subcell Biochem*. 21:95–119.
May JA, Ratan H, Glenn JR, Lösche W, Spangenberg P, Heptinstall S. 1998. GPIIb-IIIa antagonists cause rapid disaggregation of platelets pre-treated with cytochalasin D. Evidence that the stability of platelet aggregates depends on normal cytoskeletal assembly. *Platelets*. 9:227–232.
Miserey-Lenkei S, Chalancon G, Bardin S, Formstecher E, Goud B, Echard A. 2010. Rab and actomyosin-dependent fission of transport vesicles at the Golgi complex. *Nat Cell Biol*. 12:645–654.
Morré DJ, Mollenhauer HH. 2009. *The Golgi Apparatus: The First 100 Years*. New York: Springer Science+Business Media.
Mukherjee S, Chiu R, Leung SM, Shields D. 2007. Fragmentation of the Golgi apparatus: An early apoptotic event independent of the cytoskeleton. *Traffic*. 8:369–378.
Mukhopadhyay S, Linstedt AD. 2011. Identification of a gain-of-function mutation in a Golgi P-type ATPase that enhances Mn2+ efflux and protects against toxicity. *Proc Natl Acad Sci USA*. 108:858–863.
Munro S. 2011. What is the Golgi apparatus, and why are we asking? *BMC Biol*. 9:63.
Müsch A, Cohen D, Rodriguez-Boulan E. 1997. Myosin II is involved in the production of constitutive transport vesicles from the TGN. *J Cell Biol*. 138:291–306.
Myhill N, Lynes EM, Nanji JA, Blagoveshchenskaya AD, Fei H, Carmine Simmen K, Cooper TJ, Thomas G, Simmen T. 2008. The subcellular distribution of calnexin is mediated by PACS-2. *Mol Biol Cell*. 19: 2777–2788.
Nagai K, Ihara Y, Wada Y, Taniguchi N. 1997. N-glycosylation is requisite for the enzyme activity and Golgi retention of N-acetylglucosaminyltransferase III. *Glycobiology*. 7:769–776.
Niimura Y, Moue T, Takahashi N, Nagai K. 2010. Modification of sphingoglycolipids and sulfolipids in kidney cell lines under heat stress: Activation of monohexosylceramide synthesis as a ceramide scavenger. *Glycobiology*. 20:710–717.
Nilsson T, Rabouille C, Hui N, Watson R, Warren G. 1996. The role of the membrane-spanning domain and stalk region of N-acetylglucosaminyltransferase I in retention, kin recognition and structural maintenance of the Golgi apparatus in HeLa cells. *J Cell Sci*. 109:1975–1989.
Okamoto M, Yoko-o T, Miyakawa T, Jigami Y. 2008. The cytoplasmic region of alpha-1,6-mannosyltransferase Mnn9p is crucial for retrograde transport from the Golgi apparatus to the endoplasmic reticulum in *Saccharomyces cerevisiae*. *Eukaryot Cell*. 7:310–318.
Osman N, McKenzie IF, Mouhtouris E, Sandrin MS. 1996. Switching amino-terminal cytoplasmic domains of alpha(1,2)fucosyltransferase and alpha (1,3)galactosyltransferase alters the expression of H substance and Galalpha(1,3)Gal. *J Biol Chem*. 271:33105–33109.
Palmer DJ, Helms JB, Beckers CJ, Orci L, Rothman JE. 1993. Binding of coatomer to Golgi membranes requires ADP-ribosylation factor. *J Biol Chem*. 268:12083–12089.
Paulson JC, Colley KJ. 1989. Glycosyltransferases. Structure, localization, and control of cell type-specific glycosylation. *J Biol Chem*. 264:17615–17618.
Petrosyan A, Ali MF, Cheng PW. 2012. Glycosyltransferase-specific Golgi targeting mechanisms. *J Biol Chem*. 287:37621–37627.
Petrosyan A, Ali MF, Verma SK, Cheng H, Cheng PW. 2012. Non-muscle myosin IIA transports a Golgi glycosyltransferase to the endoplasmic reticulum by binding to its cytoplasmic tail. *Int J Biochem Cell Biol*. 44:1153–1165.
Petrosyan A, Britan A. 2006. Lectin-enzyme assay as a method of estimation of immunoglobulins glycosylation. *Ukrainskiĭ biokhimicheskiĭ zhurnal*. 78:151–159.
Petrosyan A, Kharchenko V. 2006. Activity of blood serum proteinases and inhibitors of proteinases as an index of gastric cancer patients' severity. *Oncologiya*. 9:303–306.
Pokrovskaya ID, Willett R, Smith RD, Morelle W, Kudlyk T, Lupashin VV. 2011. Conserved oligomeric Golgi complex specifically regulates the maintenance of Golgi glycosylation machinery. *Glycobiology*. 21:1554–1569.
Prorok-Hamon M, Notel F, Mathieu S, Langlet C, Fukuda M, El-Battari A. 2005. N-glycans of core2 beta(1,6)-N-acetylglucosaminyltransferase-I (C2GnT-I) but not those of alpha(1,3)-fucosyltransferase-VII (FucT-VII) are required for the synthesis of functional P-selectin glycoprotein ligand-1 (PSGL-1): Effects on P-, L- and E-selectin binding. *Biochem J*. 391:491–502.

Quintero CA, Valdez-Taubas J, Ferrari ML, Haedo SD, Maccioni HJ. 2008. Calsenilin and CALP interact with the cytoplasmic tail of UDP-Gal:GA2/GM2/GD2 beta-1,3-galactosyltransferase. *Biochem J*. 412:19–26.

Ropp PA, Little MR, Cheng P-W. 1991. Mucin biosynthesis: Purification and characterization of a mucin N-acetylglucosaminyltransferase. *J Biol Chem*. 266:23863–23871.

Rosso S, Bollati F, Bisbal M, Peretti D, Sumi T, Nakamura T, Quiroga S, Ferreira A, Cáceres A. 2004. LIMK1 regulates Golgi dynamics, traffic of Golgi-derived vesicles, and process extension in primary cultured neurons. *Mol Biol Cell*. 15:3433–3449.

Sakata N, Phillips TE, Dixon JL. 2001. Distribution, transport, and degradation of apolipoprotein B-100 in HepG2 cells. *J Lipid Res*. 42:1947–1958.

Schaub BE, Berger B, Berger EG, Rohrer J. 2006. Transition of galactosyltransferase 1 from trans-Golgi cisterna to the trans-Golgi network is signal mediated. *Mol Biol Cell*. 17:5153–5162.

Scheel J, Pepperkok R, Lowe M, Griffiths G, Kreis TE. 1997. Dissociation of coatomer from membranes is required for brefeldin A-induced transfer of Golgi enzymes to the endoplasmic reticulum. *J Cell Biol*. 137:319–333.

Sciaky N, Presley J, Smith C, Zaal KJ, Cole N, Moreira JE, Terasaki M, Siggia E, Lippincott-Schwartz J. 1997. Golgi tubule traffic and the effects of brefeldin A visualized in living cells. *J Cell Biol*. 139:1137–1155.

Siddhanta A, Radulescu A, Stankewich MC, Morrow JS, Shields D. 2003. Fragmentation of the Golgi apparatus. A role for beta III spectrin and synthesis of phosphatidylinositol 4,5-bisphosphate. *J Biol Chem*. 278:1957–1965.

Stamnes MA, Rothman JE. 1993. The binding of AP-1 clathrin adaptor particles to Golgi membranes requires ADP-ribosylation factor, a small GTP-binding protein. *Cell*. 73:999–1005.

Stow JL, Fath KR, Burgess DR. 1998. Budding roles for myosin II on the Golgi. *Trends Cell Biol*. 8:138–141.

Straight AF, Cheung A, Limouze J, Chen I, Westwood NJ, Sellers JR, Mitchison TJ. 2003. Dissecting temporal and spatial control of cytokinesis with a myosin II Inhibitor. *Science*. 299:1743–1747.

Togo T, Steinhardt RA. 2004. Nonmuscle myosin IIA and IIB have distinct functions in the exocytosis-dependent process of cell membrane repair. *Mol Biol Cell*. 15:688–695.

Turner JR, Tartakoff AM. 1989. The response of the Golgi complex to microtubule alterations: The roles of metabolic energy and membrane traffic in Golgi complex organization. *J Cell Biol*. 109:2081–2088.

Uliana AS, Giraudo CG, Maccioni HJ. 2006. Cytoplasmic tails of SialT2 and GalNAcT impose their respective proximal and distal Golgi localization. *Traffic*. 7:604–612.

Valderrama F, Durán JM, Babià T, Barth H, Renau-Piqueras J, Egea G. 2001. Actin microfilaments facilitate the retrograde transport from the Golgi complex to the endoplasmic reticulum in mammalian cells. *Traffic*. 2:717–726.

Vazhappilly R, Wee KS, Sucher NJ, Low CM. 2010. A non-muscle myosin II motor links NR1 to retrograde trafficking and proteasomal degradation in PC12 cells. *Neurochem Int*. 56:569–576.

Wang Q, Shen B, Zheng P, Feng H, Chen L, Zhang J, Zhang C, Zhang G, Teng J, Chen J. 2010. Silkworm coatomers and their role in tube expansion of posterior silkgland. *PLoS One*. 5:e13252.

Ward TH, Polishchuk RS, Caplan S, Hirschberg K, Lippincott-Schwartz J. 2001. Maintenance of Golgi structure and function depends on the integrity of ER export. *J Cell Biol*. 155:557–570.

Wassler MJ, Foote CI, Gelman IH, Shur BD. 2001. Functional interaction between the SSeCKS scaffolding protein and the cytoplasmic domain of beta1,4-galactosyltransferase. *J Cell Sci*. 114:2291–2300.

Waters MG, Serafini T, Rothman JE. 1991. 'Coatomer': A cytosolic protein complex containing subunits of non-clathrin-coated Golgi transport vesicles. *Nature*. 349:248–251.

Whitehouse C, Burchell J, Gschmeissner S, Brockhausen I, Lloyd KO, Taylor-Papadimitriou J. 1997. A transfected sialyltransferase that is elevated in breast cancer and localizes to the medial/trans-Golgi apparatus inhibits the development of core-2-based O-glycans. *J Cell Biol*. 137:1229–1241.

Yamaguchi N, Fukuda MN. 1995. Golgi retention mechanism of beta-1,4-galactosyltransferase. Membrane-spanning domain-dependent homodimerization and association with alpha- and beta-tubulins. *J Biol Chem*. 270:12170–12176.

Yokota S, Kitahara M, Nagata K. 2000. Benzylidene lactam compound, KNK437, a novel inhibitor of acquisition of thermotolerance and heat shock protein induction in human colon carcinoma cells. *Cancer Res*. 60:2942–2948.